Long-range diatomic s + p potentials of heavy rare gases

Long-range diatomic $s+p$ potentials of heavy rare gases

M. R. Doery, E. J. D. Vredenbregt, J. G. C. Tempelaars, H. C. W. Beijerinck, and B. J. Verhaar
Department of Physics, P.O. Box 513, Eindhoven University of Technology, 5600 MB Eindhoven, The Netherlands
(Received 14 April 1997; revised manuscript received 14 August 1997)

We examine the long-range part of the rare-gas diatomic potentials that connect to the $R\{(n-1)p^5ns\}+R\{(n-1)p^5np\}$ atomic states in the separated atom limit ($n=3$, 4, 5, and 6 for Ne, Ar, Kr, and Xe, respectively). We obtain our potentials by diagonalization of a Hamiltonian matrix containing the atomic energies and the electric dipole-dipole interaction, with experimentally determined parameters (atomic energies, lifetimes, transition wavelengths, and branching ratios) as input. Our numerical studies focus on Ne and Kr in this paper, but apply in principle to all other rare gases lacking hyperfine structure. These diatomic potentials are essential for applications in which homonuclear rare-gas pairs interact at large internuclear separations, greater than about 20 Bohr radii. Among such applications are the study of cold atomic collisions and photoassociative spectroscopy. [S1050-2947(98)07605-7]

PACS number(s): 34.20.Mq, 34.20.Cf, 32.80.Pj

I. INTRODUCTION

The increasing use of atomic traps as an experimental and technological tool [1] has kindled a keen interest in collisions at ultralow temperature. ''Bad'' collisions place a limit on trap densities, leading to signal loss (see Ref. [2], and references therein). ''Good'' collisions allow evaporative cooling of trapped atoms, the key to reaching the degenerate quantum regime in which Bose-Einstein condensation (BEC) is observed [3,4]. Aside from these issues, cold collisions are of interest in themselves as a fundamental quantum mechanical phenomenon: pure s-wave scattering can only be understood correctly as a quantum mechanical effect [5,6].

The new technique of ultracold photoassociative spectroscopy (PAS) has been used, with considerable success, to determine atomic properties of the alkali-metal atoms [7–16], and is equally appropriate for studies of the rare gases. Our own experimental efforts in this direction [17,18], as well as those of others [19–24], motivate our theoretical work on cold collisions among such atoms. As a first step towards predicting photoassociative spectra, we have investigated the long-range parts of the heavy rare-gas diatomic potentials $R\{ns\}+R\{np\}$, where $R=$ Ne, Ar, Kr, and Xe and $n=3$, 4, 5, and 6, respectively. This configuration is of particular interest because all the rare gases have metastable $R\{ns\}$ states that are likely ''ground states'' for atom trapping and cooling. Most of the fine-structure energy levels in the $R\{ns\}$ and $R\{np\}$ configurations are connected by optical transitions, $R\{ns\}\leftrightarrow R\{np\}$. In samples of trapped ''ground state'' (metastable) $R\{ns\}$ atoms, it is therefore possible to do spectroscopy of the *excited* $R\{ns\}+R\{np\}$ configurations that are the subject of this paper.

There are a few limitations to our treatment of the rare-gas diatomic potentials in this article. First and most important, we are considering only the interaction that is strongest at large internuclear separations R. Our treatment does not take into account short-range diatomic forces, such as exchange forces, or the very long-range Casimir-Polder retardation effect; see Sec. III A for a full discussion of the region of validity of our potentials. Third, the effect due to a nuclear magnetic moment (hyperfine structure) has not been considered here. Since the most abundant rare-gas isotopes lack hyperfine structure [25], this is not a serious limitation. Finally, we do not consider two of the rare gases in this article: He and Rn. Helium is an exceptional case among the rare gases, having a $1s$ core, with a $2s$ or $2p$ valence electron. While, in principle, our calculations would apply equally well to He, the notation and level schemes would all be different. The treatment of Rn is problematic because of the apparent lack of necessary experimental data, and our calculations are based in experimentally obtained quantities, as will be explained in Sec. III C.

Aside from these few limitations, our numerical calculations are applicable to any of the homonuclear rare-gas diatomic systems. Since their energy-level schemes are all similar, in this paper we concentrate when appropriate on just two example systems, Ne (Sec. V) and Kr (Sec. VI). In Sec. II we discuss differences between the rare-gas atomic systems and the alkali-metal atomic systems, since the latter have been under much study, both theoretically and experimentally, as a subject for laser cooling and trapping. Theoretical background is given in Sec. III and the method of calculating the diatomic rare-gas potentials, with some analysis, is presented in Sec. IV. Conclusions are presented in Sec. VIII.

II. THE HEAVY RARE-GAS ATOMS: A BRIEF OVERVIEW

A. Rare-gas atoms at low temperature

Most attention to the study of rare-gas atoms at low temperatures has focused on metastable helium, which was shown to be a good candidate for Bose-Einstein condensation [26], but there is no *a priori* reason to have lower expectations of the heavier rare gases. To assess the possibilities, it will be necessary to investigate their collisional properties experimentally in the same way as is being done for alkali-metal atoms [8–11,13–16]. With the relatively new technique of photoassociative spectroscopy, very precise information about the relevant atom-atom interactions

can be obtained. In this way it should be possible to determine, e.g., scattering lengths for the various rare-gas elements.

Out of the many rare-gas isotopes available, one may expect several to form stable and others to form unstable Bose condensates. In addition, there are abundant stable isotopes of Kr and Xe with half-integral total angular momenta, which would form degenerate Fermi gases at sufficiently low temperature. In order for experiments in this area to be successful, Penning ionization due to binary collisions must be suppressed. In He it has been shown that a suppression factor of 10^5 can be reached in samples that are fully stretched in electronic spin angular momentum [26,27]. In other rare gases, the situation is as yet unclear. Nevertheless, it remains true that the fully stretched states are forbidden to ionize due to spin selection rules, for any of the rare gases. Such states have both the maximum possible J, L, and S, as well as the maximum possible projection of angular momentum onto the axis of quantization. Ionization occurs when a valence electron fills up the hole in one of the $R\{(n-1)p^5\}$ cores. With fully stretched-state atoms, however, the available electron state in the core has the opposite spin from the valence electron. Hence, the spin of this valence electron would have to flip in order to fill the hole, a process that is forbidden by the usual process of Penning ionization. Spin flip then occurs only through less effective processes such as the spin-dipole interaction [26,27] and the spin-orbit interaction.

Photoassociative spectroscopy is a particularly useful tool for studying ionization, since the widths of observed levels are directly related to the ionization probability and the atomic lifetimes. In fact, in our studies we have found that several other diatomic states exist with somewhat suppressed ionization rates. Such states should have spectral lines that are narrow enough for observation in PAS experiments.

B. Rare-gas versus alkali-metal atoms: Experimental aspects

Cold collisions of alkali-metal atoms have attracted much attention [7–16], while such collisions among rare-gas atoms have been somewhat neglected [22–24,28]. This is true despite the fact that the rare gases are model atomic systems, playing an important role in fundamental atomic physics, as well as in technological applications. The principal reason for this neglect appears to be the relative experimental ease of building and operating an optical trap for alkali-metal atoms. Optical transitions in alkali-metal atoms may be excited from the ground state with ordinary lasers, so that a trap can be produced within a vapor cell. In contrast, excitation of the rare-gas atoms is not easily possible via optical transitions from the ground state, since this requires extreme-ultraviolet lasers.

Fortunately for atom trappers, two of the first-excited $R\{(n-1)p^5ns\}$ states are metastable, and can be used as effective ground states in laser cooling processes ($R=$Ne, . . . ,Xe for $n=3, \ldots ,6$). From there, transitions via optical excitation to the $R\{(n-1)p^5np\}$ states are possible. Unfortunately, the usual method of metastable production using a plasma discharge is an inefficient process: at best, only about 1 in 10^3 atoms exiting the source are in the metastable state [29]. This provides a poor starting point for the experimentalist attempting to optically cool and trap these atoms.

Furthermore, if the source is situated near the trapping region, collisions with the high-energy, background atoms occur too frequently to maintain a dense trap. Such collisions are already problematic in alkali-metal traps, but in a metastable rare-gas trap the proportion of atoms suitable for trapping (namely, metastables) relative to background is much smaller, as already mentioned. This means that a gas cell containing the metastable source is generally not well suited for a rare-gas trap [30]. Instead, metastables must be cooled and slowed after production, and only then loaded into a trap, leading to a rather complicated experimental setup. Yet another difficulty comes from trap loss through ionizing collisions (this is in addition to the usual collision-induced losses, that are known to occur in alkali-metal traps [31,32]). Ionization-induced loss is estimated to be of about the same order of magnitude as collision-induced losses among the alkalis [2]. Finally, the finite lifetime of the metastables, on the order of several tens of seconds, places a limit to the amount of time spent by an individual atom in the trap [33,34].

C. Rare-gas versus alkali atoms: Theoretical aspects

The rare gases differ from the alkalis in that, as a general rule, the most abundant isotopes have total nuclear spin equal to zero, so hyperfine structure is not present [25]. The extensive hyperfine structure of most alkalis severely complicates the theoretical description of low-temperature collisions [11]. One simple reason for this is that it increases the number of states involved in a homonuclear, diatomic molecule by a factor $(2I+1)^2$ where I is the nuclear spin quantum number. Here, I ranges from $\frac{3}{2}$ for ^{23}Na, among others, to $\frac{7}{2}$ for ^{133}Cs. Second and more important, since the hyperfine splitting is generally of the same order of magnitude as the kinetic energy in cold collisions, it also influences the collision dynamics through angular momentum decoupling and recoupling phenomena [11–13,16].

On the other hand, singly excited rare-gas atoms are complicated by extensive fine structure. The valence electronic structure of a singly excited rare-gas atom is the same as that of the ground state of an alkali atom, for which the ns or np valence electron alone produces the electronic term structure. In the case of alkali atoms, there are one ns ($^2S_{1/2}$) and two np ($^2P_{1/2,3/2}$) nondegenerate fine-structure states; counting degenerate magnetic sublevels makes a total of two ns and six np states (neglecting hyperfine structure). For the rare-gas atoms, in addition, the angular momentum of the $(n-1)p^5$ core couples to that of the ns or np valence electron, so that more terms result. The spin and orbital quantum numbers of the core, $l_c=1$ and $s_c=\frac{1}{2}$ lead to an increase in the number of terms by a factor of 6. There are then four energy levels in the ns configuration, which add up to a total of 12 atomic states when degenerate magnetic sublevels are taken into account; the np configuration has ten energy levels, for a total of 36 magnetic sublevels (see Fig. 1).

A quick calculation reveals how very many diatomic potentials are possible for the rare gases, when only the subset of $\{ns\}$ and $\{np\}$ states are included: $(12+36)^2=2304$. This number is quite comparable to a typical case with alkali atoms: for ^{23}Na with $I=\frac{3}{2}$, the number is 1024. The main difference is then that the asymptotic energy differences be-

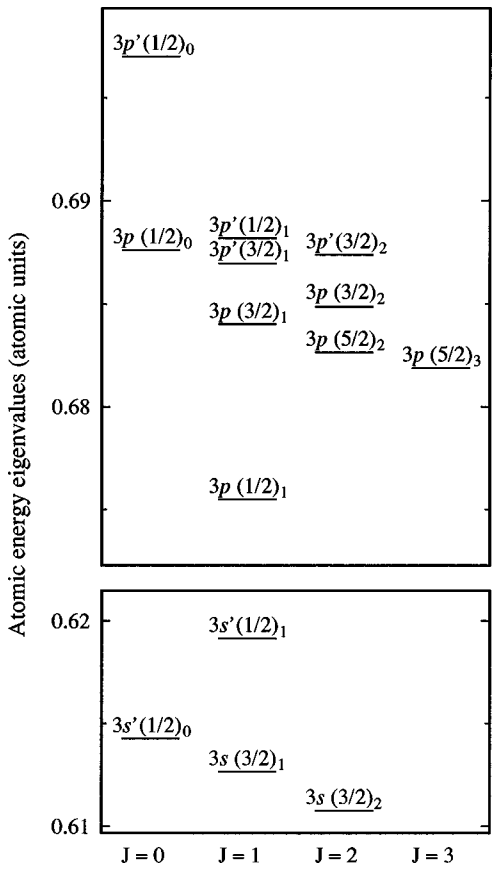

FIG. 1. Energy eigenvalues of atomic Ne, $3s$ and $3p$ configurations. Energies are given relative to the Ne $2p^6$ ground state, and states are labeled with intermediate coupling J_c-ℓ (Racah) notation.

tween the diatomic states are in general much larger for the rare gases. Hyperfine splittings of the ground-state ns in the alkali-metal atoms are typically several GHz; those of the first-excited np state are even smaller. This should be contrasted with the fine-structure splittings of the ns and np states in the rare gases, which are typically thousands of GHz. This shifts the complications in the theoretical treatment from long range for alkalis [11,15] to short range for the rare gases. In the case of the alkalis, long-range complications have been circumvented by working with carefully chosen potentials, such as doubly spin-polarized states [8], or states with no hyperfine splitting [8,16].

D. Spectroscopic notation and selected atomic properties

The energy spacings of the excited states of the rare gases have all been experimentally obtained (for Ne and Kr, these energies are given in Table I, and have been taken from Refs. [35,36]). The states, written as $n\ell(K)_J$ or $n\ell'(K)_J$, are identified in J_c-ℓ notation (also known as intermediate coupling or Racah notation). The angular momentum $\vec{K}$ is defined by $\vec{K}=\vec{J}_c+\vec{\ell}$, where J_c is the total electronic angular momentum quantum number of the core, ℓ is the orbital angular momentum quantum number of the valence electron, and J is the total electronic angular momentum of the atom. A configuration marked with a prime originates from the $(n-1)p^5(^2P_{1/2})$ core; unprimed configurations originate from the $(n-1)p^5(^2P_{3/2})$ core. It should be emphasized that generally only J is a good quantum number for any of these states. It so happens that the ns states with $J=0$ or 2, and the np state with $J=3$, also have well-defined L and S (total electronic orbital and spin angular momentum, respectively). Therefore these states may also be denoted as $(n-1)p^5(ns\ ^3P_0)$, $(n-1)p^5(ns\ ^3P_2)$, and $(n-1)p^5(np\ ^3D_3)$, following Russell-Saunders (L-S coupling) notation.

Atomic lifetimes for decay from levels in the Ne and Kr ns and np configuration are also given in Table I. Note that only the $ns'(1/2)_0$ and $ns(3/2)_2$ states are metastable. The branching ratios $B_{k\to k'}$ for transitions of the sort $R(np)\to R(ns)$, between energy levels k and k', are given in Tables II and III, for Ne and Kr.

III. HAMILTONIAN FOR LONG-RANGE INTERACTION OF HEAVY RARE GASES

A. Regions of validity for the long-range interaction

Population of very long-range diatomic bound states by photoassociative techniques is an experimental reality [14,15], with varied applications. We are interested in describing such states that may be populated by optical excitation during collisions that occur at large internuclear separations in a beam or trap of metastable $\{ns\}$ atoms. We now address what is meant by ''long range'' here.

The dominant interaction between two neutral, homonuclear atoms at sufficiently large internuclear separation is the Van der Waals interaction ([37], p. 1130 ff). When the two atoms have different energies, $E_1\neq E_2$, this is referred to as the *resonant* electric dipole-dipole interaction; when they have the same energy, $E_1=E_2$, it is called the *induced* electric dipole-dipole interaction. Several authors have treated the dipole-dipole interaction between a ground-state alkali-metal atom and an excited alkali-metal atom [38,39], but to our knowledge this situation has not yet been explored in the rare-gas systems.

At short range, the van der Waals interaction is not suitable for description of interatomic interactions, where the overlap of the electron charge distributions leading to interatomic repulsion is not negligible. A crude estimate of the expectation value of the radial position, $\overline{r_n}$, of an outer n-shell electron of a many-electron atom is given by a simplified Hartree model [40]:

$$\overline{r_n}\approx n a_0, \tag{1}$$

where the Bohr radius $a_0=0.529\times10^{-10}$ m. In Ref. [40], this result is said to overestimate the correct number by about a factor of 2. Then for the overlap of electron clouds to be negligible, internuclear separations R should be somewhat larger than this average distance, $R\gg\overline{r_n}$. In Ne, with $n=3$, this means $R\gg\overline{r}_{n=3}\approx3a_0$, while in Xe, it requires $R\gg\overline{r}_{n=6}\approx6a_0$. Forces due to electron cloud overlap are not included in our treatment, so its validity is then restricted to R greater than about $10a_0$ or $20a_0$. See Sec. V C for further details.

It is known that for internuclear separations on the order of the transition wavelength involved, $R_{\rm ret}\approx\hbar c/|E_2-E_1|=\lambda/2\pi$, the atom-atom interaction is affected by the delay

TABLE I. Energies E of first excited states of Ne ($n=3$) and Kr ($n=5$) relative to the ground state, $(n-1)p^6$. Neon energies are taken from Ref. [35], while Kr energies are taken from Ref. [36] (more digits are given in these references). Notation is J_c-ℓ coupling; see Sec. II D. Note that the Ne energies are ordered according to energy, while for Kr there is some disorder in this respect. Radiative lifetimes $1/\Gamma=\tau$ for these states are also given. Unless noted otherwise, lifetimes of Ne are taken from Ref. [59]; for Kr, lifetimes were taken from Ref. [60] when possible, because of the reported accuracy of their measurements.

State $n\ell(K)_J$	Ne energy (a.u.)	Ne $1/\Gamma$	Kr energy (a.u.)	Kr $1/\Gamma$
$ns'(1/2)_1$	0.61916	1.70 ns[a]	0.39115	3.87 ns[a]
$ns'(1/2)_0$	0.61428	430 s[b]	0.38816	0.488 s[b]
$ns(3/2)_1$	0.61264	12.8 ns[a]	0.36868	4.31 ns[a]
$ns(3/2)_2$	0.61074	24.4 s[b]	0.36438	38 s[c]
$np'(1/2)_0$	0.69699	14.5 ns[d]	0.45042	22.1 ns[e]
$np'(1/2)_1$	0.68818	18.28 ns	0.44615	23.5 ns[e]
$np(1/2)_0$	0.68763	17.38 ns	0.42872	23.5 ns[f]
$np'(3/2)_2$	0.68736	18.69 ns	0.44627	28.5 ns[e]
$np'(3/2)_1$	0.68697	19.05 ns	0.44468	29.5 ns[e]
$np(3/2)_2$	0.68489	19.38 ns	0.42430	27.35 ns
$np(3/2)_1$	0.68400	19.49 ns	0.42358	29.51 ns
$np(5/2)_2$	0.68265	19.56 ns	0.42058	32.10 ns
$np(5/2)_3$	0.68189	19.42 ns	0.42052	27.73 ns
$np(1/2)_1$	0.67551	25.43 ns[g]	0.41539	40.0 ns[h]

[a]Reference [70].
[b]Reference [61]. But see the caveat in Ref. [34], and also see following footnote.
[c]Reference [71].
[d]Reference [72].
[e]Reference [62]. More recent but less complete data are found in Ref. [63].
[f]Reference [73].
[g]Reference [64].
[h]Reference [63].

due to the finite speed of light [41,42]. Transition wavelengths for $R\{ns\}$ to $R\{np\}$ vary, but satisfy $\lambda>500$ nm. The effects of this Casimir-Polder retarded interaction then play a small role for $R\lesssim 1500a_0$, which is an approximate upper bound on R for the region of validity of our treatment.

B. Unperturbed Hamiltonian

At infinitely large internuclear separation, $R=\infty$, the total energy of an isolated, two-atom system is just the sum of the individual, unperturbed atomic energies,

$$E_{\text{asymp}}=E_1+E_2, \quad R\to\infty. \tag{2}$$

Here, E_i is the atomic energy of atom i in an individual energy level in the $n\ell$ configuration, as given in Table I for Ne and Kr. The quantum mechanical Hamiltonian for the two separated atoms is then

$$H_0=H_1+H_2, \tag{3a}$$

$$H_i=\sum_k E_k \sum_{M_J} |k,J_k,M_J\rangle_{i\ i}\langle k,J_k,M_J|, \tag{3b}$$

for $i=1,2$. The atomic Hamiltonians H_i are diagonal operators whose elements are the atomic energies E_k. The label k identifies the atomic state, which may be any of the four ns or ten np orbitals (the restriction of our basis set is discussed in Sec. VII A). The total electronic angular momentum of that state, J_k, is also given, along with the projection of J_k onto the internuclear axis, M_J.

The eigenvectors $|a\rangle$ of the unperturbed Hamiltonian H_0 are solutions of the equation $H_0|a\rangle=E_a|a\rangle$. Since H_0 is diagonal in the basis of product states of atomic states, these are the eigenvectors:

TABLE II. Branching ratios [65] $B_{k\to k'}$ (%), for transitions Ne$(3p)\to$Ne$(3s)$. Values are not listed when the transition is electric dipole forbidden. Reference [64] also gives values for these branching ratios that are very similar to those presented here.

$nl'(K)_J$	$3p'(1/2)_0$	$3p'(1/2)_1$	$3p(1/2)_0$	$3p'(3/2)_2$	$3p'(3/2)_1$	$3p(3/2)_2$	$3p(3/2)_1$	$3p(5/2)_2$	$3p(5/2)_3$	$3p(1/2)_1$
$3s'(1/2)_1$	98.65	42.23	1.37	43.08	43.46	34.00	3.74	5.93		0.33
$3s'(1/2)_0$		26.94			48.11		20.09			6.29
$3s(3/2)_1$	1.35	10.05	98.63	33.73	1.30	7.89	64.26	58.33		25.70
$3s(3/2)_2$		20.79		23.19	7.13	58.12	11.91	35.74	100.00	67.68

TABLE III. Branching ratios [66], $B_{k\to k'}$ (%), for transitions Kr($5p$)→Kr($5s$). Values are not listed when the transition is electric dipole forbidden.

$nl'(K)_J$	$5p'(1/2)_0$	$5p'(1/2)_1$	$5p(1/2)_0$	$5p'(3/2)_2$	$5p'(3/2)_1$	$5p(3/2)_2$	$5p(3/2)_1$	$5p(5/2)_2$	$5p(5/2)_3$	$5p(1/2)_1$
$5s'(1/2)_1$	99.24	43.10	0.00	96.60	51.91	1.03	0.43	0.41		0.47
$5s'(1/2)_0$		52.78			47.96		0.20			0.67
$5s(3/2)_1$	0.76	0.25	100.00	2.80	0.12	25.56	85.95	69.74		12.42
$5s(3/2)_2$		3.87		0.60	0.01	73.41	13.42	29.85	100.00	86.44

$$|a\rangle = |k, J_k, M_J\rangle_1 |k', J'_{k'}, M'_{J'}\rangle_2 . \quad (4)$$

We will call these individual product states the ''unperturbed diatomic basis,'' because they are the eigenstates of H_0, the Hamiltonian at $R=\infty$.

C. Interaction term

When two atoms are sufficiently separated so that their charge distributions do not overlap, the interaction between them can be expressed in a multipole expansion, which has the form of a power series in $1/R$ [43,44]. For two neutral atoms, the first nonzero term in this expansion is associated with the electrostatic dipole-dipole interaction. The classical expression for the interaction between two electric dipoles is

$$W_{d\text{-}d} = \frac{1}{4\pi\varepsilon_0 R^3}[\vec{d}_1 \cdot \vec{d}_2 - 3(\vec{d}_1 \cdot \vec{u}_R)(\vec{d}_2 \cdot \vec{u}_R)]. \quad (5)$$

The electric dipole moments $\vec{d}_1$ and $\vec{d}_2$ are expressed as $\vec{d} = -e\Sigma_l \vec{r}_l$, where the sum over l is a sum over the position vectors of all electrons relative to the nucleus of the atom considered. The permittivity of vacuum is given by $\varepsilon_0 = 8.85\times10^{-12}$ F m^{-1}, and $e = 1.602\times10^{-19}$ C is the elementary charge. The unit vector $\vec{u}_R$ points from the center of the first dipole to the center of the second one.

In many of the excited states that we are considering in this paper, rare-gas atoms have a nonvanishing quadrupole moment. This is due to the existence of incompletely filled $(n-1)p$ and/or np shells. As a result, and in contrast to the case of alkali atoms, the next first-order term in the multipole expansion is the quadrupole-quadrupole term, with behavior [67]

$$W_{q\text{-}q} = C_5/R^5. \quad (6)$$

While it would be possible to include this term in the Hamiltonian that we consider in this paper, we have found it to be quite small in the expected R range of validity of our potentials, discussed in Sec. III A. A detailed treatment has shown that compared to the first- ($\propto R^{-3}$) and second-order ($\propto R^{-6}$) perturbations due to the dipole-dipole interaction, the quadrupole-quadrupole interaction is generally a minor effect. We therefore postpone the discussion of its expected order of magnitude and its effect on the calculated potential curves to Sec. VII.

For the states considered in this paper, which contain incomplete electron shells with angular momentum quantum number l no greater than one (i.e., only s and p orbitals), all higher multipole terms vanish in a first-order treatment (see, e.g., Refs. [67] and [37], p. 1059 ff) and will therefore not be considered.

Quantizing $\vec{d}_i$ in Eq. (5) results in the following expression for the dipole-dipole interaction ([37], p. 1130 ff):

$$W_{d\text{-}d} = -\frac{1}{4\pi\varepsilon_0 R^3}[\hat{d}_{1,+}\hat{d}_{2,-} + \hat{d}_{1,-}\hat{d}_{2,+} + 2\hat{d}_{1,0}\hat{d}_{2,0}]. \quad (7)$$

The interaction has been written in terms of the standard components of the irreducible tensor operator $\hat{d}$, of rank 1: $\hat{d}_+ = -(\hat{d}_x + i\hat{d}_y)/\sqrt{2}$, $\hat{d}_- = (\hat{d}_x - i\hat{d}_y)/\sqrt{2}$, and $\hat{d}_0 = \hat{d}_z$ ([45]). The electric dipole operators $\hat{d}_{i,\mu}$ are labeled by $i=1$ or 2 according to whether they operate on the first or second atom. The matrix elements of $\hat{d}_\mu$ can be expressed in terms of reduced dipole matrix elements, $\langle k\|\hat{d}\|k'\rangle$ through the Wigner-Eckart theorem [45]:

$$\langle kJ_kM_J|\hat{d}_\mu|k'J'_{k'}M'_{J'}\rangle = \frac{\langle k\|\hat{d}\|k'\rangle}{\sqrt{2J_k+1}}(J'_{k'}1M'_{J'}\mu|J_kM_J). \quad (8)$$

The full Hamiltonian is symbolically written as follows:

$$H = H_0 + W_{d\text{-}d}. \quad (9)$$

There are numerous parameters implicit in Eq. (9): the atomic energies of $R\{ns\}$ and $R\{np\}$ and the reduced dipole matrix elements for all electric dipole-allowed transitions. The reduced dipole matrix elements can be calculated from atomic properties: the atomic lifetime $\tau_k = 1/\Gamma_k$ of state k; the branching ratio $B_{k\to k'}$ from state k to k'; and the wavelength for that transition, $\lambda_{k\to k'}$. The expression is as follows [45]:

$$|\langle k\|d\|k'\rangle| = \sqrt{3\pi\varepsilon_0\hbar\left(\frac{\lambda_{k\to k'}}{2\pi}\right)^3 \Gamma_{k\to k'}(2J_{k'}+1)}. \quad (10)$$

The notation $\Gamma_{k\to k'} = B_{k\to k'}\Gamma_k$ has been used.

Values of the atomic properties needed for the explicit evaluation of Eq. (9) have been determined in experimental studies of the rare gases. Atomic energies have already been listed in Table I for Ne and Kr. Other experimental values are taken from the literature and are repeated here in Tables II and III, for Ne and Kr (wavelengths were calculated from energies and have not been tabulated here). In our numerical calculations, we use these experimentally obtained values of these atomic properties (the exception being the Kr branching ratios, which were theoretically determined). Our pri-

mary interest in the $R\{ns\}$-$R\{np\}$ diatomic potentials is in the calculation of low-energy collision problems, which can be described predominantly in terms of the long-range parts of the potentials [9,46]. Therefore we have not attempted an *ab initio* determination of these potentials, as would be required for an accurate description of chemical bonding forces between atoms at short range.

IV. ANALYSIS OF THE HAMILTONIAN

A. Block diagonalization of the Hamiltonian

The total Hamiltonian of Eq. (9) is not diagonal in the unperturbed diatomic basis. Nevertheless, the matrix elements of H are conveniently evaluated within it: the matrix elements of H_0 are just sums of atomic energies, and the matrix elements of $W_{d\text{-}d}$ are expressed in terms of products of reduced dipole matrix elements with Clebsch-Gordan coefficients.

Before beginning any computations, it pays to take a close look at the interaction term $W_{d\text{-}d}$, which is entirely off-diagonal. The dipole operator produces excitation or deexcitation. Thus, in Eq. (7), the products of dipole operators for the individual atoms require that the interaction permits only the following types of connections:

$$|s\rangle_1|p\rangle_2 \leftrightarrow |p\rangle_1|s\rangle_2, \tag{11a}$$

$$|s\rangle_1|s\rangle_2 \leftrightarrow |p\rangle_1|p\rangle_2. \tag{11b}$$

In each of these cases, $\ell = s$ or p, and the $\Delta\ell = \pm 1$ selection rule [25] holds for each individual atom. The notation has been shortened, so that $|\ell\rangle$ is used to mean an individual fine-structure level in the $n\ell$ configuration. Forbidden connections are of the sort

$$|s\rangle_1|p\rangle_2 \not\leftrightarrow |p\rangle_1|p\rangle_2. \tag{12}$$

A restriction of our basis set is implicit in Eqs. (11) and (12). Only $R\{ns\}$ and $R\{np\}$ states ($R = \mathrm{Ne}, \ldots, \mathrm{Xe}$; $n = 3, \ldots, 6$, respectively) are included in our calculations. Other states $\{n'\ell\}$ where $n' \neq n$ have been excluded. This restriction is investigated in Sec. VII A.

Connections of the type given in Eq. (11a) are consistent with the *resonant* electric dipole-dipole interaction. This interaction is proportional to the inverse of the third power of the internuclear separation ($\propto R^{-3}$). If atom 1 is in an s orbital, atom 2 must be in a p orbital and vice versa, expressing conservation of parity. For a physical picture, one might imagine atom 1 in a p orbital releasing a (virtual) photon in the process of making a transition to the s level; atom 2 absorbs the photon and is excited to the corresponding p state. The two atoms behave like coupled harmonic oscillators.

The connections given in Eq. (11b) are of the type described by the *induced* electric dipole-dipole interaction. In this case, either both atoms are in the s state or both are in the p state. In a semiclassical description, the negatively charged electrons move about the positively charged nucleus, so that each atom has a fluctuating dipole moment. The dipole of one atom is the source of an electric field that induces a dipole moment in the other atom; the interaction between the two momentarily formed dipoles is proportional to the inverse of the sixth power of the internuclear separation ($\propto R^{-6}$).

The only types of transitions allowed by the dipole-dipole interaction are indicated in Eqs. (11a) and (11b). This is also seen if the interaction is written in symbolic form:

$$W_{d\text{-}d} = \begin{pmatrix} \begin{pmatrix} 0 & {}_1\langle s|_2\langle p|W|p\rangle_1|s\rangle_2 \\ {}_1\langle p|_2\langle s|W|s\rangle_1|p\rangle_2 & 0 \end{pmatrix} & \begin{pmatrix} 0 & 0 \\ 0 & 0 \end{pmatrix} \\ \begin{pmatrix} 0 & 0 \\ 0 & 0 \end{pmatrix} & \begin{pmatrix} 0 & {}_1\langle s|_2\langle s|W|p\rangle_1|p\rangle_2 \\ {}_1\langle p|_2\langle p|W|s\rangle_1|s\rangle_2 & 0 \end{pmatrix} \end{pmatrix}. \tag{13}$$

The interaction matrix is thus conveniently split into two uncoupled blocks. (Each of the ''matrix elements'' of these blocks is in itself a block matrix.) The upper-left block contains the matrix elements described by Eq. (11a), while the lower-right block contains matrix elements described by Eq. (11b). The form of this matrix makes it clear that eigenstates of the resonant dipole-dipole interaction do not mix with those of the induced dipole-dipole interaction. In this article, we are interested in finding eigenfunctions of the resonant dipole-dipole interaction. At sufficiently large R, these are the states that give the potentials on which an excited p-state rare-gas atom collides with its metastable partner. Therefore we will pay no further attention to the lower-right block in Eq. (13), but instead focus on the upper-left block.

Closer inspection of the dipole-dipole interaction yields another conservation rule. As indicated in Eq. (7), the products of dipole operators in $W_{d\text{-}d}$ always act to conserve $M_1 + M_2$, the sum of the projections of $\vec{J}_1$ and $\vec{J}_2$. Once again, only transitions of a certain sort are allowed:

$$|J,M\rangle_1|J',M'\rangle_2 \leftrightarrow |J'',M''\rangle_1|J''',M'''\rangle_2$$
$$(\text{forbidden unless } M + M' = M'' + M'''). \tag{14}$$

(Implicit are the usual electric dipole selection rules for J.) We define $\Omega = |M_1 + M_2|$. States with differing Ω do not couple, and consequently the Hamiltonian is block diagonal in Ω. Considering values of $\Omega < 0$ is redundant because these states are not essentially different from those with $\Omega > 0$. The change in sign of Ω is equivalent to a reflection in a plane containing the internuclear axis (quantization axis); for this reason, Ω is usually taken to be non-negative ([47], Chap. V.2).

TABLE IV. Number of matrix elements in each Ω block.

Ω	0	1	2	3	4	5
No. of elements	192	166	106	48	14	2

Diagonalizing the Hamiltonian has now become somewhat simplified. There are $12\times36\times2=864$ product states of $R\{ns\}$ with $R\{np\}$, when all fine-structure levels are included, each having a well-defined J, with its complement of $2J+1$ degenerate magnetic sublevels. The multiplicative factor of 2 comes about because there are two possible permutations, $|s\rangle_1|p\rangle_2$ and $|p\rangle_1|s\rangle_2$. Discarding all states with $\Omega'<0$ leaves a total of 528 states. When the matrix is made block diagonal in Ω, each block is considerably smaller; as an example, the $\Omega=5$ case produces a 2×2 matrix. The sizes of the other matrices are presented in Table IV.

B. Evaluation and diagonalization of Hamiltonian matrix

The computation of the eigenvalues and eigenvectors of H is made considerably easier by block diagonalization. To obtain diatomic potentials, each block of the Hamiltonian is first numerically evaluated at a specific value of R. Eigenvalues and eigenvectors of the separate blocks of the Hamiltonian are found by a numerical matrix diagonalization routine [48]. A new value of R is chosen and the procedure is repeated, to obtain the R dependence of the diatomic potentials. These states may be labeled according to their inversion symmetry (g or u), as well as their reflection symmetry ($+$ or $-$) in the case $\Omega=0$ [47,49]. These symmetries are determined from the eigenvectors found in the diagonalization procedure.

C. General form of the diatomic potentials and numerical tests

Block diagonalization of the Hamiltonian makes the eigenvalue problem considerably smaller. Ideally, one would diagonalize the Hamiltonian analytically to find expressions for the diatomic potentials $V(R)$ in closed form. Realistically, diagonalization of most of the blocks is only feasible numerically. Nevertheless, one can gain some insight into the potentials by exploring the Hamiltonian further.

Potentials obtained using the full system are expressed as an expansion in powers of R^{-3}, since in the approximation made in Sec. III C the R^{-5} term due to the quadrupole-quadrupole interaction is absent (the validity of this approximation is investigated in Sec. VII B). As a general rule, therefore,

$$V(R)=C_0+\frac{C_3}{R^3}+\frac{C_6}{R^6}+\cdots . \tag{15}$$

The term C_3R^{-3} results from electric dipole-allowed couplings. This can be seen by examining a truncated atomic system, with only two fine-structure levels of different parity, having total angular momentum J_1 and J_2, and energies E_1 and E_2. For such a system, at $R<\infty$, a whole manifold of potential curves approach the asymptotic energy of the separated atoms, $E_{\text{asymp}}=E_1+E_2$. The transition $J_1\leftrightarrow J_2$ is dipole allowed, so $|J_1-J_2|=1$ or 0 (excluding $J_1=J_2=0$). The Hamiltonian for this truncated system is written in symbolic matrix form as

$$H_{\text{trunc}}=(E_1+E_2)I+W_{d\text{-}d}, \tag{16}$$

where I is the identity matrix, and all the matrix elements of $W_{d\text{-}d}$ are off-diagonal and proportional to R^{-3}. Since all the diagonal elements are equal, it is easy to show that the eigenvalues have an R dependence that is purely inverse cubic. Couplings to yet another state (or states) of different energy (energies) introduces the higher-order terms, such as R^{-6}, present in Eq. (15).

The coefficients in Eq. (15) are obtained by numerically fitting the computed R dependence of the eigenvalues of H to such a power series [50]. Each potential curve of the manifold of states connecting to E_{asymp} can be expressed in this way. In order to obtain accurate numerical values of C_3 alone, one diagonalizes the truncated system as given in Eq. (16). Numerically, it is easier to fit the potentials resulting from such a truncated basis, since they have a pure R^{-3} dependence, in principle. Including all four ns and ten np states of the full basis set results in higher-order terms, which necessarily increase the complications for a numerical fitting routine.

Since values of C_3 can be found from the truncated basis alone, ''reduced C_3 coefficients'' C_3^{red} may be obtained. These coefficients are numerical factors that do not depend on atomic properties, so that they are identical for all the rare-gas atoms. They need only be multiplied by a factor F_n that depends only on the electric dipole matrix elements $\langle ns\|\hat{d}\|np\rangle$, or equivalently on the transition probabilities, wavelengths, and branching ratios for individual states, which differ from one rare-gas species to another. The value of C_3 for a particular rare-gas system is obtained by using

$$C_3=F_nC_3^{\text{red}}, \tag{17a}$$

$$F_n=\lambda_{k\rightarrow k'}^3\Gamma_{k\rightarrow k'}, \tag{17b}$$

where k stands for the $|np\rangle$ state and k' is the $|ns\rangle$ state. A tabulation of C_3^{red} for all of the hundreds of diatomic potentials would be quite lengthy, so this is not done here.

D. Special case: Laser cooling transition

As stated in the Introduction, we have a special interest in the potential curves connecting asymptotically with the $ns(3/2)_2+np(5/2)_3$ separated atomic states, because these atomic states form the cycling transition that is used for cooling and trapping. There are 40 potential curves connecting asymptotically to this separated atom limit: 10, 10, 8, 6, 4, and 2 curves for $\Omega=0$, 1, 2, 3, 4, and 5, respectively.

Of all these potentials, the $\Omega=5$ case is especially interesting. In this case, the Hamiltonian block is exactly 2×2, with no dipole-dipole coupling to any other states. Therefore these potentials have exactly $1/R^3$ behavior, as is easily seen to occur when diagonalizing a matrix of the sort

$$H=\begin{pmatrix} E & \Delta/R^3 \\ \Delta/R^3 & E \end{pmatrix}. \tag{18}$$

The two solutions consist of one attractive and one repulsive potential, $V(R)=E+C_3/R^3$, with $C_3=\pm\Delta$. The attractive potential curve has u symmetry, and can therefore be excited from an $\Omega=4$ ''ground state,'' $ns(3/2)_2+ns(3/2)_2$, which has g symmetry.

Also, recall that metastable rare gases can easily be lost from atomic traps in ionizing collisions. But the $\Omega=5$ diatomic states are made up of internal angular momentum states that are forbidden to ionize, due to spin selection rules. This is seen by examining the associated eigenfunctions, which are particularly simple:

$$|5_g\rangle=\frac{1}{\sqrt{2}}[|(ns)2,2\rangle_1|(np)3,3\rangle_2+|(np)3,3\rangle_1|(ns)2,2\rangle_2], \tag{19a}$$

$$|5_u\rangle=\frac{1}{\sqrt{2}}[|(ns)2,2\rangle_1|(np)3,3\rangle_2-|(np)3,3\rangle_1|(ns)2,2\rangle_2]. \tag{19b}$$

Individual kets on the right-hand side of Eqs. (19) are total angular momentum states for each atom, $|(n\not{\ell})J,M\rangle_i$. The components are products of atomic states that are fully stretched in both spin and orbital electronic angular momentum: They have both the maximum possible J, L, and S, as well as the maximum possible projection of angular momentum onto the internuclear axis. As explained in Sec. II A, ionization is severely suppressed for such states. Out of all the possible states, the $\Omega=5$ case is the only one where this is true.

Reduced C_3 coefficients for the $ns(3/2)_2+np(5/2)_3$ manifold have been obtained using the method described in Sec. IV C. All but two of the fine-structure energy levels were removed from the Hamiltonian, retaining *only* the $ns(3/2)_2$ and $np(5/2)_3$ atomic states, so all of the potential curves follow perfectly R^{-3} power laws. The reduced coefficients can be used to obtain C_3 values for all potential curves in this manifold, when multiplied by a factor F_n [see Eq. (17a)] that depends only on the electric dipole matrix elements for a specific rare-gas atom, $\langle ns(3/2)_2\|\hat{d}\|np(5/2)_3\rangle$. These reduced coefficients are presented in Table V. The calculated values of $\langle ns(3/2)_2\|\hat{d}\|np(5/2)_3\rangle$ and F_n for this specific manifold are listed in Table VI, for Ne, Ar, Kr, and Xe, together with the wavelengths and lifetimes used for the calculations.

E. Diatomic lifetimes

Once the eigenvectors $|\xi\rangle$ of the diatomic states have been determined, their lifetimes $1/\Gamma_\xi$ can also be found. The matrix elements of $\hat{d}_{1,\mu}+\hat{d}_{2,\mu}=\hat{d}_{\mathrm{tot},\mu}$ between these diatomic states and the diatomic ''ground states,'' $|s\rangle_1|s\rangle_2$, are calculated, squared, and summed to obtain these lifetimes:

$$\Gamma_\xi=\sum_{k,k'}\sum_{M_J,M_{J'}}\sum_{\mu}|_1\langle kJ_kM_J|_2\langle k'J'_{k'},M_{J'}|\hat{d}_{\mathrm{tot},\mu}|\xi\rangle|^2. \tag{20}$$

Here, the sum over k and k' is now only a sum over $R\{ns\}$ states; $R\{np\}$ states are excluded.

TABLE V. Values of C_3 obtained from truncated basis $ns(3/2)_2+np(5/2)_3$ for Ne_2 and Kr_2 ($n=3,5$ respectively) and reduced values C_3^{red} valid for all $R=$Ne, . . . ,Xe. Spontaneous decay rates of diatomic states, Γ_ξ, are given in terms of Γ_k, the spontaneous decay rate of the $np(5/2)_3$ atomic state in this example.

State	Ne_2 C_3 (a.u.)	Kr_2 C_3 (a.u.)	10^7 C_3^{red} (hartree a_0^3 ns/nm^3)	Γ_ξ/Γ_k
0_u^+	−10.42	−14.84	−7.701	1.323
0_g^-	−7.725	−11.01	−5.712	1.000
0_u^+	−5.677	−8.090	−4.198	1.217
0_g^-	−3.845	−5.480	−2.843	1.000
0_u^+	−3.487	−4.969	−2.578	1.060
0_g^+	3.487	4.969	2.578	0.940
0_u^-	3.845	5.480	2.843	1.000
0_g^+	5.677	8.090	4.198	0.783
0_u^-	7.725	11.01	5.712	1.000
0_g^+	10.42	14.84	7.701	0.677
1_u	−10.28	−14.64	−7.598	1.264
1_g	−7.523	−10.72	−5.562	0.869
1_u	−5.280	−7.524	−3.904	1.045
1_g	−4.057	−5.781	−3.000	0.845
1_u	−0.028	−0.041	−0.021	1.005
1_g	0.028	0.041	0.021	0.995
1_u	4.057	5.781	3.000	1.155
1_g	5.280	7.524	3.904	0.955
1_u	7.523	10.72	5.562	1.131
1_g	10.28	14.64	7.598	0.736
2_u	−9.856	−14.05	−7.288	1.302
2_g	−6.879	−9.803	−5.086	0.992
2_u	−4.490	−6.398	−3.320	1.198
2_g	−0.348	−0.496	−0.257	0.974
2_u	0.348	0.496	0.257	1.026
2_g	4.490	6.398	3.320	0.802
2_u	6.879	9.803	5.086	1.008
2_g	9.856	14.05	7.288	0.698
3_u	−9.144	−13.03	−6.761	1.387
3_g	−5.756	−8.202	−4.256	0.854
3_u	−1.507	−2.147	−1.114	1.200
3_g	1.507	2.147	1.114	0.800
3_u	5.756	8.202	4.256	1.146
3_g	9.144	13.03	6.761	0.613
4_u	−8.112	−11.56	−5.998	1.230
4_g	−3.662	−5.218	−2.708	0.897
4_u	3.662	5.218	2.708	1.104
4_g	8.112	11.56	5.998	0.771
5_u	−6.675	−9.512	−4.936	2.000
5_g	6.675	9.512	4.936	0.000

In general, the diatomic state eigenvectors vary with R, so that the diatomic lifetimes are also a function of R. At large R, these eigenvectors vary only slightly, and the diatomic lifetimes approach a constant value. Table V contains the diatomic state lifetimes for all the states in the truncated system that was discussed in Sec. IV D. These diatomic state lifetimes were determined as written in Eq. (20), at $R=100a_0$, and are expressed in terms of the atomic state lifetime. For this truncated system, the eigenvectors do not

TABLE VI. Wavelengths λ (*in vacuo*), lifetimes τ, and derived reduced dipole matrix elements for transitions $R(^3P_2)\leftrightarrow R(^3D_3)$. The conversion factor F_n may be used to obtain approximate values of C_3 for all rare-gas species. (See text.)

Atom	λ (nm)	τ (ns)	$\langle ^3P_2\|d\|^3D_3\rangle$ (ea_0)	$10^{-7}\ F_n$ (nm^3/ns)
^{20}Ne	640.402[a]	19.42[b]	5.777	1.352
^{40}Ar	811.754[a]	33.1[c]	6.14	1.62
^{84}Kr	811.513[d]	27.73[e]	6.896	1.927
^{136}Xe	882.184[f]	34[g]	7.06	2.02

[a]Reference [35].
[b]Reference [59].
[c]Reference [74].
[d]Reference [36].
[e]Reference [60].
[f]Reference [75].
[g]Reference [76].

depend on the particular rare-gas system being considered. These diatomic lifetimes are then good for any of the heavy rare-gas diatomic molecules in the $ns(3/2)_2+np(5/2)_3$ manifold. Their values range from half the value of the atomic lifetime to infinity.

V. APPLICATION TO Ne

In the following discussion of specific diatomic potentials, certain concepts repeatedly arise that deserve special notation. Every pair of atomic states gives rise to a *manifold* of potentials. For each pair of atomic states, the sum of the energies of these atomic states, each measured from the single atomic ground state, is the asymptotic energy $E_{\rm asymp}=E_1+E_2$. [It should be noted that this is the coefficient C_0 in Eq. (15).] An attractive potential has a minimum (well) of depth $V_{\rm min}$ that is located at internuclear separation $R_{\rm min}$. The value of $V_{\rm min}$ is given in terms of its difference from $E_{\rm asymp}$. The inner turning point $R_{\rm in}$ for such a potential is the smallest value of R that satisfies $V(R)-E_{\rm asymp}=0$.

A word about units is also in order. In atomic units, the hartree is the unit of energy, 1 hartree=27.2 eV, and the Bohr radius $a_0=0.529\times10^{-10}$ m is the unit of distance. Hence, when C_3 is given in a.u., it should be clear that this means hartree a_0^3. In some cases, when speaking of a laser detuning, it is also useful to give a frequency, e.g., 1 GHz corresponds to 1.52×10^{-7} a.u. References [51,33] contain useful conversion factors and discussions of units.

A. Diatomic Ne potentials: inverse cubic potentials

The potentials for diatomic Ne have been calculated numerically, using the method described in Sec. IV B. These potentials are presented separately, for different values of Ω, in Fig. 2. A general pattern is evident at first: the potential curves at the lowest energies are forced downward, due to couplings with the large number of states with the same symmetry above them, while those at the highest energies are forced upward. Within the cluster of potentials in the center, crossings and avoided crossings appear at shorter range ($R\lesssim30a_0$). Avoided crossings provide opportunities for fine-structure changing collisions, which is another trap-loss mechanism in addition to ionization. In some cases, these avoided crossings produce ''humps'' in attractive potentials [a hump is a region where $V(R)>E_{\rm asymp}$]. Such potentials may support quasibound states. In this complicated inner region, one also finds attractive potentials with wells and steep, repulsive walls. Naturally, these are not perfect representations of the true short-range potentials, since at smaller internuclear distances contributions from exchange forces compete with the dipole-dipole interaction (see Sec. III A). Nevertheless, it is clear that there are both pitfalls and opportunities at small R. The pitfalls stem from the complications in dealing with such a tangle of potentials, while the opportunities can be found in this rich structure with so many phenomena available for investigation.

At long range ($R\gtrsim30a_0$), the potential curves smoothly approach their asymptotic limits. If a potential stems from a pair of atomic states that are connected by a dipole-allowed transition, the long-range behavior is of the form R^{-3}. If the transition is dipole forbidden, then $C_3=0$, and the long-range behavior is of the form R^{-6} to lowest order. This has been verified by numerically fitting [50] the potential curves to the first three terms in Eq. (15), in the region $50a_0\lesssim R\lesssim500a_0$. Even when the asymptotic atomic states are connected by a dipole-allowed transition, nonexistent branching ratios between the two asymptotic atomic states can result in potentials with R^{-6} behavior. Such potentials generally appear almost constant at long range, on the scale of the figures.

The magnitudes of C_3 for these many potentials vary by several orders of magnitude. A fairly small value, $C_3\approx10^{-2}$ a.u., is found in the $\Omega=1$ manifold of the Ne $3s(3/2)_2+$Ne $3p'(3/2)_1$ state, located at $E_{\rm asymp}=1.2977$ a.u. The largest is $C_3=10.4$ a.u., and is found in an $\Omega=0$ state of the Ne $3s(3/2)_2+$Ne $3p(5/2)_3$ manifold ($E_{\rm asymp}=1.2926$ a.u.). In fact, for every value of Ω, the largest values of C_3 are all found in the Ne $3s(3/2)_2+$Ne $3p(5/2)_3$ state. This comes about because this $J=2\leftrightarrow J=3$ transition involves the largest possible Clebsch-Gordon coefficient, 1, and a relatively large dipole transition matrix element (due to the 100% branching ratio).

B. Diatomic Ne potentials: inverse sixth potentials

Some of the diatomic potentials shown in Fig. 2 have $C_3=0$, so that in the approximation made in Sec. III C where the R^{-5} term due to the quadrupole-quadrupole interaction is neglected, they are actually of the form C_6R^{-6} in lowest order (the validity of this approximation is investigated in Sec. VII B). An interesting example of this occurs for two of the $\Omega=2$ curves in the Ne $3s(3/2)_2+$Ne $3p(5/2)_2$ manifold ($E_{\rm asymp}=1.2934$ a.u.). The two eigenvectors can be written

$$|2_u\rangle=\frac{1}{2}[|(3s)2,0\rangle_1|(3p)2,2\rangle_2-|(3s)2,2\rangle_1|(3p)2,0\rangle_2 -|(3p)2,0\rangle_1|(3s)2,2\rangle_2+|(3p)2,2\rangle_1|(3s)2,0\rangle_2], \tag{21a}$$

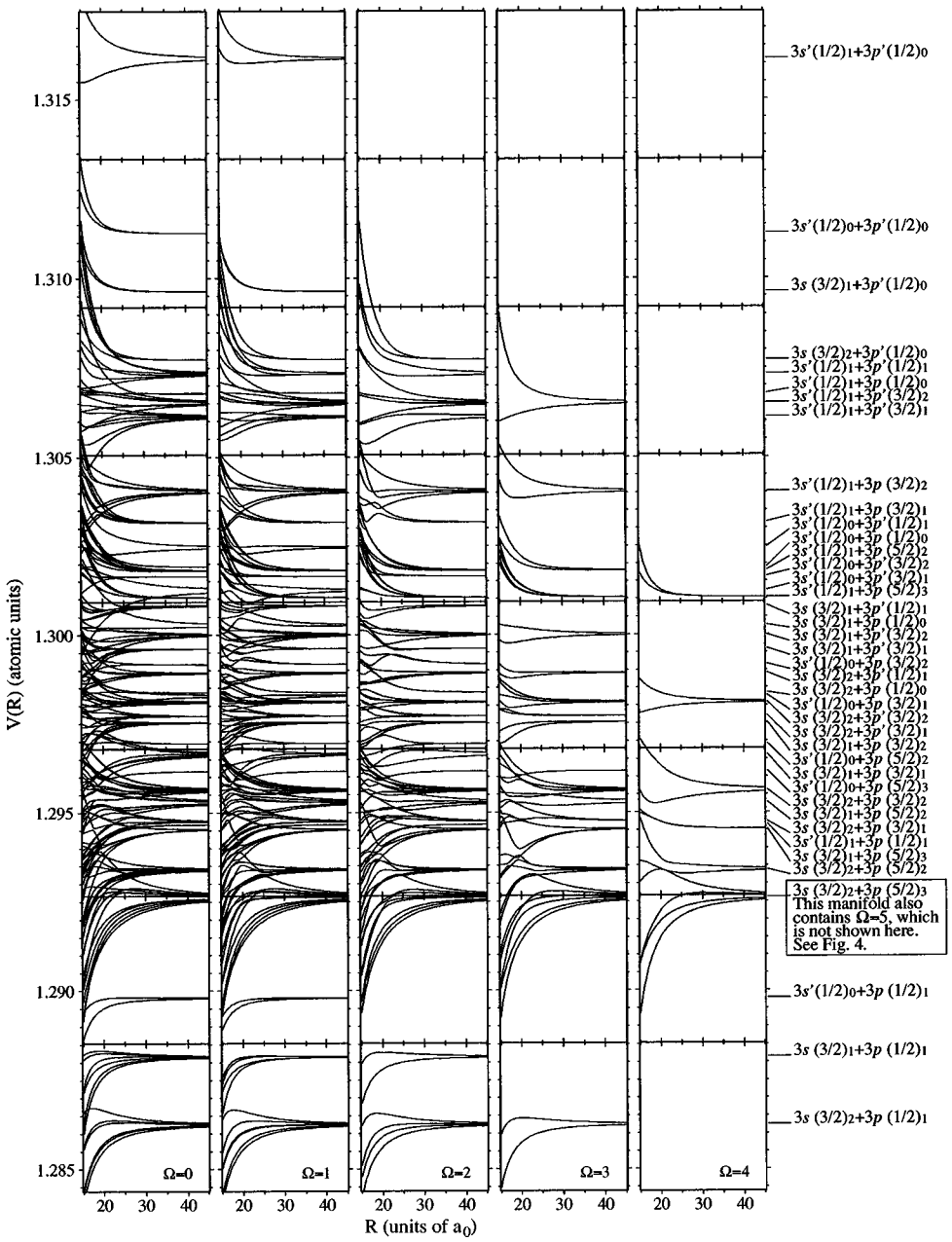

FIG. 2. Diatomic Ne potentials, $\Omega=0,\ldots,4$ (see Fig. 4 for $\Omega=5$).

$$|2_g\rangle=\frac{1}{2}[|(3s)2,0\rangle_1|(3p)2,2\rangle_2-|(3s)2,2\rangle_1|(3p)2,0\rangle_2 +|(3p)2,0\rangle_1|(3s)2,2\rangle_2-|(3p)2,2\rangle_1|(3s)2,0\rangle_2], \tag{21b}$$

where the notation used in Eqs. (19) is also used here. The states in Eqs. (21) are unusual in consisting entirely of dipole-forbidden connections (because $|M_1-M_2|=2>1$). Stated mathematically, $\langle 2_u|W_{d\text{-}d}|2_u\rangle=0$, and the same holds for $|2_g\rangle$.

As another example of an R^{-6} potential, we turn to the diatomic state Ne $3s'(1/2)_0$+Ne $3p'(3/2)_2$, located at $E_{\text{asymp}}=1.3016$ a.u. The variation in these potentials is only visible at $R\lesssim 30a_0$. A numerical fit to these curves produces C_3 coefficients that are practically zero, $|C_3|<10^{-5}$ a.u., while their C_6 coefficients are typical for all of these curves, on the order of 10^4 a.u. The transition $J'=2\leftrightarrow J=0$ is dipole forbidden, so matrix elements of the form ${}_1\langle 3s'(1/2)_0|_2\langle 3p'(3/2)_2|W_{d\text{-}d}|3p'(3/2)_2\rangle_1|3s'(1/2)_0\rangle_2$ are exactly zero, and these diatomic states are connected only in second order, resulting in $C_3=0$.

When C_3 is very small and negative, a positive value of C_6 can result in very shallow attractive potentials with minima at fairly large R. An example is the Ne $3s'(1/2)_1$ +Ne $3p(1/2)_0$ state, at $E_{\text{asymp}}=1.3068$ a.u. All values of C_3 associated with this manifold are on the order of only 10^{-2} a.u., while $|C_6|$ is on the order of 10^4 or 10^5 a.u.; for these potentials $V_{\min}$ is on the order of 1 to 0.1 GHz, with $R_{\min}$ located at tens of a_0. While the transition $J=1\leftrightarrow J'=0$ is dipole allowed, the branching ratio between these two atomic states is almost zero, as shown in Table II. It should be noted that many of the dipole-allowed transi-

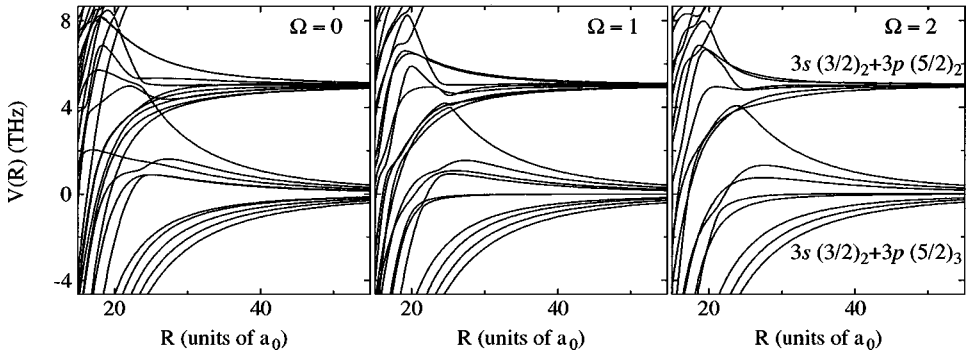

FIG. 3. Diatomic Ne potentials connecting asymptotically to $3s(3/2)_2+3p(5/2)_3$ and $3s(3/2)_2+3p(5/2)_2$ limits (asymptotic energies are 1.2926 a.u. and 1.2933 a.u., respectively): $\Omega=0,1,2$. The $3s(3/2)_2+3p(5/2)_3$ asymptotic limit has been chosen as the zero of energy, here.

tions have very small branching ratios. This follows from the general rule for the heavy rare gases that transitions that preserve the state of the core, J_c, are strongly preferred (this is by no means an exact selection rule, however). Thus $s'\leftrightarrow p$ and $s\leftrightarrow p'$ transitions have low branching ratios.

Unfortunately, the values of C_6 quoted are not expected to be exact. These values of C_6 result from second-order contributions to the dipole-dipole interaction between $R\{ns\}$ and $R\{np\}$ states alone. Further contributions to C_6 must come from states that are higher in energy, $R\{(n+1)p\},R\{(n+2)p\},\ldots$, etc. These higher-energy terms have not been included in our calculations, but should produce only small corrections to our potential curves (see Sec. VII A). The values of C_3 are not affected by this problem, since only a single pair of atomic states contributes to their value, as pointed out in Sec. IV C.

C. Diatomic Ne potentials: Estimate of behavior at short range

The potentials are somewhat unreliable at short range, where overlap of the electron clouds of the two atoms becomes significant. An estimate of approximately where this takes place was given in Sec. III A; for Ne the overlap should be large at around $R=3a_0$. A better estimate is necessary to determine where chemical bonding effects begin to become important. To our knowledge, the chemical structure of the excited Ne_2 diatomic molecule, $Ne\{ns\}+Ne\{np\}$, has not been calculated. Excited Na_2 *has* been investigated extensively, however. The latter differs from Ne_2 due to its filled core, but its valence electron occupies the same orbital. Assuming that chemical bonds are predominantly due to the valence electron, a good estimate of the short-range Ne_2 interaction can be obtained by studying that of Na_2.

The easiest case to work with is the 5_u state, with the Ne $3s(3/2)_2+$Ne $3p(5/2)_3$ asymptote. This can also be written Ne $3s(^3P_2)+$Ne $3p(^3D_3)$, because these states have good quantum numbers L and S; for the $3s$ Ne atom, $L=S=1$, while for the $3p$ atom, $L=2$ and $S=1$. Since the 5_u state is fully stretched in electronic spin and orbital angular momentum (see Sec. IV D), adding these angular momenta must result in maximum values of these angular momenta for the diatomic state, i.e., $L_{tot}=3$ and $S_{tot}=2$. The corresponding state in Na_2 has the Na $3s(^2S_{1/2})$ + Na $3p(^2P_{3/2})$ asymptote. The maximum values of angular momenta for a fully stretched Na_2 atom are $L_{tot}=1$ and $S_{tot}=1$, and further, the u symmetry must be preserved. The Na_2 diatomic state that most closely corresponds to our $Ne_2 5_u$ is then labeled $^3\Pi_u$. Excited Na_2 potentials have been calculated by Konowalow *et al.* and later by Jeung [52]. At $R=15a_0$, the Konowalow potential has a depth of -0.0024 a.u. and the Jeung value is -0.0020 a.u. This is to be compared with the $Ne_2 5_u$ potential, which has a depth of -0.0020 a.u. at $R=15$. Differences are due to several factors: (a) the overlap of the valence electrons is not included in our calculation; (b) the Ne_2 and Na_2 cores differ; and (c) our basis set is more restricted than that used in Ref. [52]. Even so, the difference between the Konowalow result and our calculated potential at $R=15a_0$ is then only 4×10^{-4} a.u., about 20%, while Jeung's result coincides with ours. Therefore we conclude that at $R\approx15a_0$ chemical bonding is fairly unimportant; furthermore, its effects drop off rapidly as R increases.

D. Laser cooling transition in Ne

As stated in the Introduction, we have a special interest in the potential curves connecting asymptotically with the Ne $3s(3/2)_2+$Ne $3p(5/2)_3$ separated atomic states, because these atomic states form the cycling transition that is used for cooling and trapping. These potential curves, 40 in all, are shown in closeup in Figs. 3 and 4. At long range, half the potentials are attractive ($C_3<0$) and half are repulsive ($C_3>0$). The latter potentials may be useful for suppression of trap-loss collisions, a mechanism that has already been studied in Xe [24,28] and Kr [23], for example. The attractive potentials support bound states that will be suitable for photoassociative spectroscopy.

The $\Omega=5$ potentials have pure R^{-3} dependence, with $|C_3|=6.7$ a.u. As explained in Sec. V C above, chemical bonding makes these potentials unreliable at internuclear separations less than about $R=15a_0$. The attractive potential 5_u is quite deep there, with $V(15a_0)=-0.0020$ a.u. In comparison, photoassociative spectroscopy is usually carried out with detunings below atomic resonance on the order of several GHz $\approx10^{-7}$ a.u. As an example, a detuning of -5 GHz will excite colliding atomic pairs to bound states of the 5_u potential at about $R=200a_0$. In contrast, the same detuning

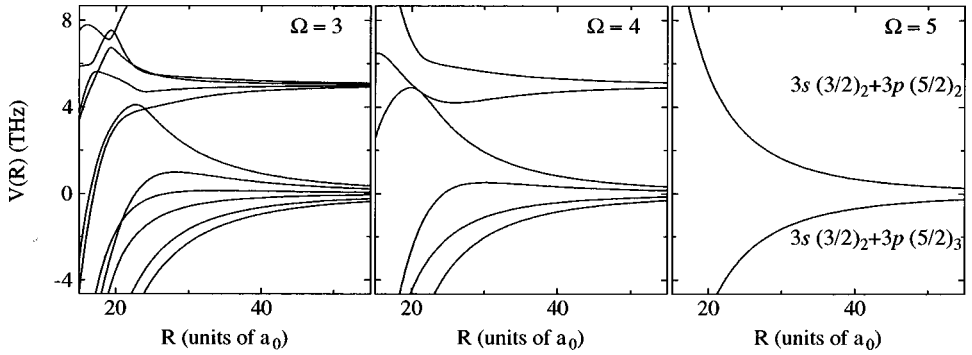

FIG. 4. Same as in Fig. 3, only for $\Omega=3,4,5$. Note that there are no $\Omega=5$ potentials in the $3s(3/2)_2+3p(5/2)_2$ manifold.

will produce excitation to bound states of the most shallow attractive 1_u state, seen in Fig. 3, at about $R=20a_0$. This state has a very small coefficient, $C_3=-10^{-2}$ a.u.

Applying laser light that is detuned close below the $3s(3/2)_2 \leftrightarrow 3p(5/2)_3$ transition to a gas of metastable Ne will excite colliding atoms to bound states in all of the 40 potentials approaching the asymptote, resulting in a complicated spectrum, with rotational and vibrational spectra from all these potentials overlapping each other. It should be possible to distinguish between the spectra because the spacing of vibrational lines due to a C_3R^{-3} potential at long range is related specifically to the value of C_3 [53,54]. Also, the rate of transitions occurring at small R will be small compared to those at large R, since the excitation cross sections scale with R^2. Another distinguishing factor is the ionization probability, which is quite large for states other than $\Omega=5$. It is possible that only the $\Omega=5$ spectrum will be distinguishable, as sharp peaks rising above the broad irresolvable ionization spectrum due to the other potentials. If the other spectra are resolvable, however, it will be possible to obtain information about ionization from the spectral line shapes. We are currently studying the ionization probabilities of these states, and will present our results elsewhere.

E. Pure long-range Ne potentials

In Fig. 2, there are several potentials that are ''pure long range.'' This is a rather loose term, which is related to the inner turning point $R_{\rm in}$. A potential is said to be *pure* long range if $R_{\rm in}$ is so large that even the inner repulsive part of the potential is well described by the long-range forces, as opposed to exchange forces, which are due to overlap of the electron charge distributions [55].

As noted in Sec. V C, exchange forces are competitive with the electric dipole-dipole interaction at $R \lesssim 15a_0$, so such pure long-range potentials must have $R_{\rm in} \gtrsim 15a_0$. For example, among the $\Omega=3$ potentials of the $3s(3/2)_2+3p'(3/2)_2$ manifold ($E_{\rm asymp}=1.2981$ a.u.), there are two attractive and two repulsive potentials. Of the attractive potentials, the higher curve has a very shallow well of $V_{\rm min}=-0.35\times10^{-5}$ a.u.$=-23$ GHz, below the asymptote, and $R_{\rm in}=31a_0$. A fit to this curve indicates that $C_3=-0.43$ a.u., and $C_6=1\times10^4$ a.u. Therefore it is apparent that this potential is pure long range because the C_6 term is competitive with the fairly small C_3 at unusually large R. In Sec. V B, it was noted that our calculated C_6 is not wholly reliable. Spectroscopic measurements of this particular state would have to be made for an experimental test of the accuracy of these values of C_6. If it is assumed that these pure long-range attractive potentials have the form $V(R)=-|C_3|R^{-3}+|C_6|R^{-6}$, a small correction to C_6, in the form of a multiplicative factor $(1+x)$ for $x \ll 1$, introduces a multiplicative correction factor of $(1+x/3)$ to $R_{\rm min}$, and $(1-x)$ to $V_{\rm min}$. For example, a 25% decrease in the value of C_6 results in about a 25% increase in the well depth; whether or not a shift in the vibrational spectrum would be detectable depends largely on the ionization widths of the levels. These widths are expected to be quite small because atoms in these states never get much closer to each other than $31a_0$. Ionization probabilities decrease exponentially with internuclear separation, and at this large distance they should be negligible.

As another example, in the $3s'(1/2)_1+3p'(1/2)_1$ manifold ($E_{\rm asymp}=1.3073$ a.u.), another shallow well ($V_{\rm min}=113$ GHz) can be found when $\Omega=0$, with $R_{\rm in}=27a_0$. Again, this well seems to result from the competition between a positive $C_6=1.5\times10^4$ a.u. and a somewhat weak, negative $C_3=-1.2$ a.u. term. Careful inspection of the large number of potential curves reveals more of these shallow, pure long-range potentials, not visible on the scale of Fig. 2.

A pure long-range potential was recently used to make an accurate measurement of the lifetime of Na$\{3s\}$ and to observe the Casimir-Polder retarded force [10]. We expect that several of the pure long-range potentials in the heavy rare gases may be useful for similar types of precision measurements. A complication in this case is that only two of the $R\{ns\}$ states are metastable, the $ns'(1/2)_0$ and $ns(3/2)_2$ states. For example, with Ne, it would then be extremely difficult to populate the particular $3s'(1/2)_1+3p'(1/2)_1$ potential just mentioned above, since it would have to be populated via excitation from the short-lived $3s'(1/2)_1$ state, which is essentially empty in any Ne gas cell or atomic beam. The $3s(3/2)_2+3p'(3/2)_2$ potential described earlier is a promising candidate, however, since it can be populated by laser excitation from a metastable state.

VI. APPLICATION TO Kr

A. Diatomic Kr potentials

The potentials for diatomic Kr are shown in Fig. 5. These potentials are similar to those for diatomic Ne. On this scale, the most notable difference is the clustering of the potentials into three groups. In the heavier rare gases, such as Kr and

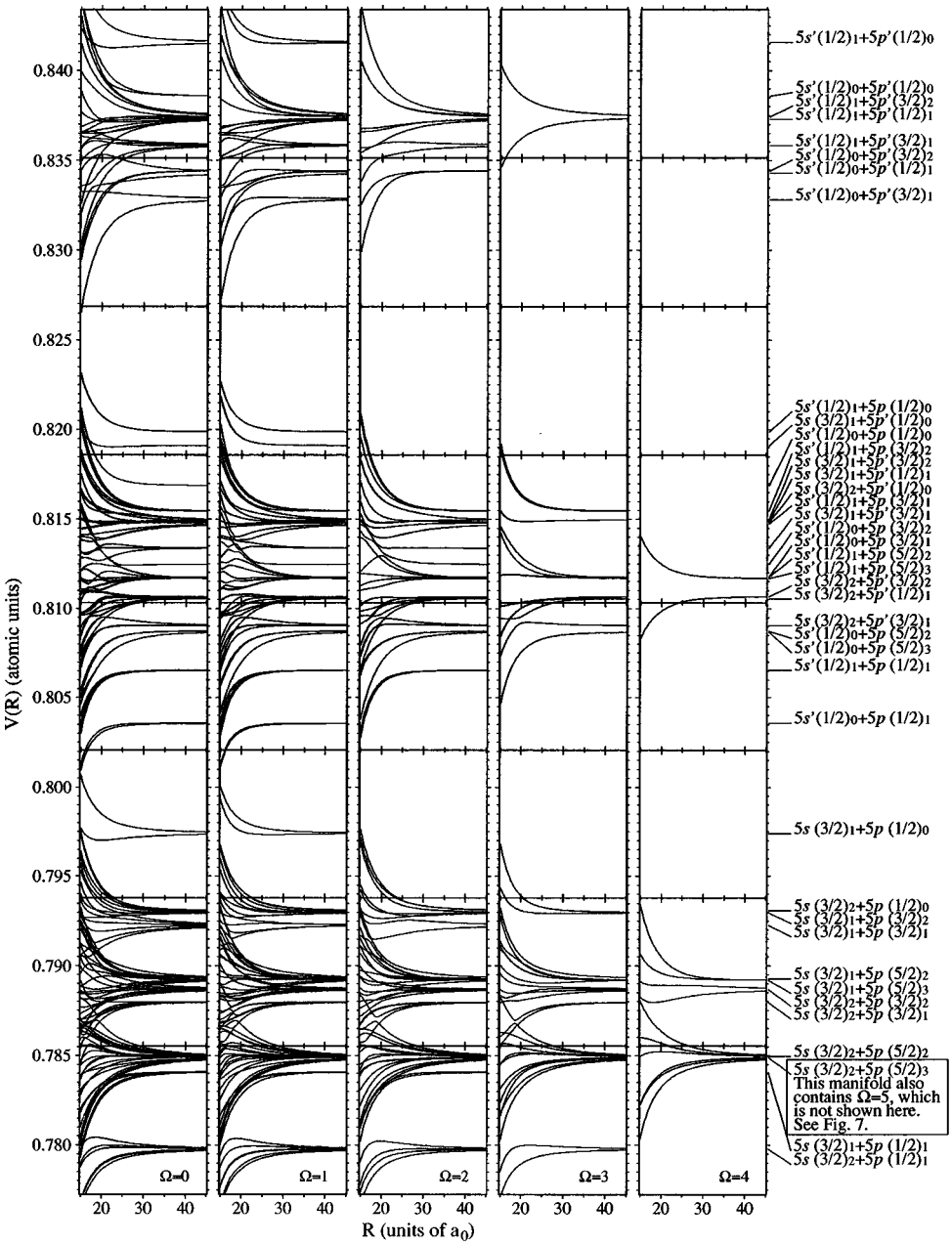

FIG. 5. Diatomic Kr potentials, $\Omega=0,\ldots,4$ (see Fig. 7 for $\Omega=5$).

Xe, the splitting between ns and ns' is more pronounced than in Ne; the same is true of the splitting between np and np'. This is the result of stronger spin-orbit coupling in the $(n-1)p^5$ core for these heavier atoms [25]. In Fig. 5, then, one sees a lower-energy group asymptotically connecting to separated atom pairs with $5s+5p$, a medium-energy group connecting to $5s'+5p$ and $5s+5p'$, and a higher-energy group connecting to $5s'+5p'$.

Otherwise, the Kr potentials appear similar to those for Ne. The potentials can be written as a power series in R^{-3}, and at smaller values of R, numerous avoided crossings can be seen, resulting in a complicated *fine-structure* ''spaghetti.''

B. Laser cooling transition in Kr

For Kr, the laser cooling transition is $5s(3/2)_2 \leftrightarrow 5p(5/2)_3$. The diatomic potentials resulting from the coupling at long range of these two separated atom states are shown in Figs. 6 and 7. The values of C_3 are tabulated in Table V, alongside those for diatomic Ne. In comparison to diatomic Ne, these curves tend to be steeper, with a maximum of $|C_3|=14.84$ a.u. This is due to the difference in the lifetimes and transition wavelengths of the $ns(3/2)_2 \leftrightarrow np(5/2)_3$ transition in Ne and Kr. Using Eq. (10), one finds that for this manifold, the C_3 coefficients for Ne are smaller than those for Kr by a factor of 0.70.

C. Pure long-range Kr potentials

Pure long-range potentials are evident in Fig. 5; for example, an $\Omega=4$ potential in the $5s(3/2)_2+5p(3/2)_2$ manifold ($E_{\text{asymp}}=0.788\,68$ a.u.) has a minimum at about $18a_0$. Even more noteworthy is the $5s(3/2)_2+5p(5/2)_2$ manifold ($E_{\text{asymp}}=0.784\,96$ a.u.). The attractive potentials are *very*

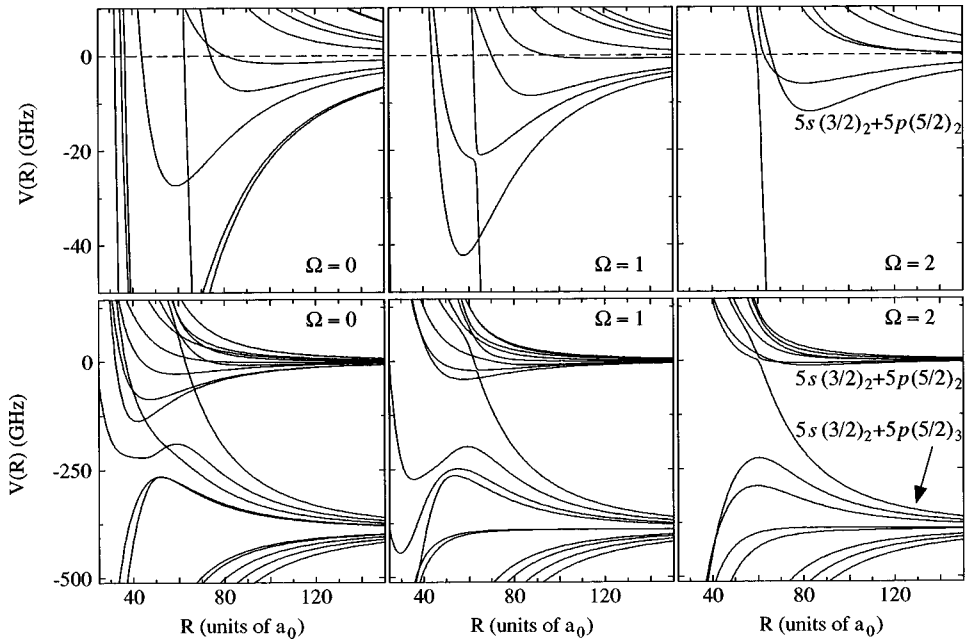

FIG. 6. Diatomic Kr potentials connecting asymptotically to $5s(3/2)_2+5p(5/2)_2$ and $5s(3/2)_2+5p(5/2)_3$ limits (asymptotic energies are 0.7850 a.u. and 0.7849 a.u., respectively), for $\Omega=0,1,2$. The $5s(3/2)_2+5p(5/2)_2$ asymptotic limit has been chosen as the zero of energy. In the upper set, the plots focus in on the $5s(3/2)_2+5p(5/2)_2$ asymptote; note the change of scale in $V(R)$.

pure long range, having minima anywhere between $R \approx 40a_0$ and $120a_0$. They are so shallow that it would not be possible to discern them clearly on the scale of Fig. 5, so an exploded view is given in Figs. 6 and 7.

These shallow potentials are the result of avoided crossings that occur when the repulsive $5s(3/2)_2+5p(3/2)_3$ potentials rise up to meet the attractive $5s(3/2)_2+5p(3/2)_2$ potentials. States of the same symmetry repel each other, so that the downward-turning attractive potentials are forced up again. Such avoided crossings occur among other states, as was shown for diatomic Ne in Sec. V E. Unlike those potentials, these particular pure long-range potentials do not result from very small, negative values of C_3 which are overwhelmed at long range by positive C_6 terms; values of C_3 range from at least $C_3=-0.55$ a.u. to at most $C_3=-4.81$ a.u. [For $\Omega=2$, there are also the two states with $C_3=0$, which have already been discussed in Sec. V A. See Eqs. (21).] In Kr, these avoided crossings occur at such long range because the $5p(3/2)_2$ is fortuitously close in energy to the $5p(3/2)_3$ state, only about 5.9×10^{-5} a.u.$=13\ \mathrm{cm}^{-1}$ away. A potential in the $5s(3/2)_2+5p(3/2)_2$ manifold having a large and negative C_3 term approaches the $5s(3/2)_2$

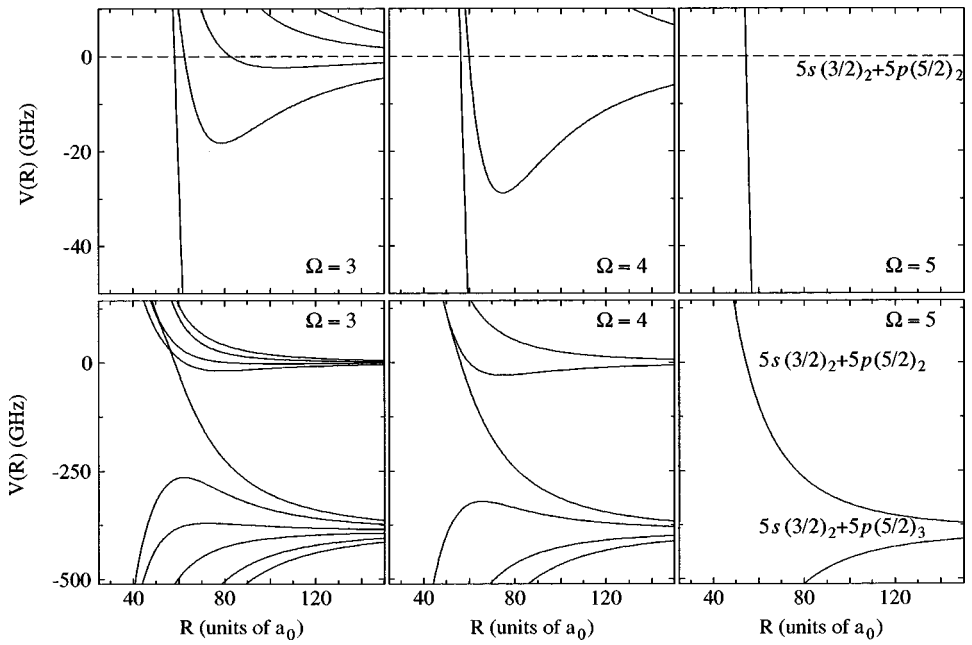

FIG. 7. Same as in Fig. 6, only for $\Omega=3,4,5$. Note that there are no $\Omega=5$ potentials in the $5s(3/2)_2+5p(5/2)_2$ manifold. There is a change of scale in $V(R)$ in the upper set of plots.

$+5p(3/2)_3$ neighboring manifold at relatively large distances, and then turns up in an avoided crossing, creating a well at large R.

The $5s(3/2)_2+5p(3/2)_2$ potentials look very promising for experimental studies of atomic properties. They are accessible via 810 nm laser excitation from the metastable $5s(3/2)_2$ state. By numerical integration of the Schrödinger equation using the method of Ref. [56], we have determined that all of these potentials have vibrational bound states, even the very shallowest one, which is in the $\Omega=1$ manifold. Photoassociative spectroscopy of these potentials should be possible with well-resolved spectra, since at such large internuclear separations, ionization is negligible.

One also expects to find similar pure long-range potentials that result from all the $5s$ and $5s'$ states connecting to the $5p(3/2)_2$ state. There are limitations to the uses of these other potentials. Such potentials connecting to the short-lived $5s'(1/2)_1$ and $5s(3/2)_1$ states are difficult to populate. And the $5s'(1/2)_0+5p(3/2)_2$ state can only be populated via a dipole-forbidden transition from the metastable $5s'(1/2)_0$ state ($J=0\leftrightarrow J=2$).

VII. LIMITATIONS

A. Restriction of basis states

As noted earlier, in the calculation of our diatomic potentials we have used a restricted basis set, $R\{ns\}$ and $R\{np\}$, $R=$Ne, . . . ,Xe and $n=3, \ldots ,6$ respectively. A more precise calculation would have to take into account contributions to the electric dipole-dipole interaction due to other states of higher energies: $R\{(n+1)p\}$, $R\{(n+2)p\}$, etc. One expects such states to have only a small effect on the shape of the potentials calculated here, because the energy difference between diatomic states $R\{ns\}+R\{(n+1)p\}$ and $R\{ns\}+R\{np\}$ is in general quite large. Furthermore, the inclusion of such states will not change the value of C_3 for a particular diatomic potential, since that depends only on the dipole matrix element for the transition between the two separated atomic states. The inclusion of higher-energy states *will* change the higher-order terms in Eq. (15), however, the C_6 terms in particular. These are important for the study of pure long-range potentials, since they are primarily responsible for the radial positions and energy depths of potential well minima, as was discussed in Sec. V E. It is then desirable to obtain an estimate of the degree to which such higher-energy states would affect the calculated potentials, if they were included. Unfortunately, such an estimate is difficult because of the scarcity of available data for transitions from higher-energy states to $R\{ns\}$. The situation has been studied in the alkali atoms, however, so we turn our attention there for the moment.

Bussery and Aubert-Frécon [57] (and more recently Marinescu and Dalgarno [58]) have calculated values of C_6 dispersion coefficients for diatomic alkali $ns+np$ molecules. They included many basis states with atomic term numbers $n'>n$. For Na, C_6 is in the range of 2 to 4×10^3 a.u., while for Rb, it is between 1 and 2×10^4 a.u. When spin-orbit coupling is included, however, potentials with C_3's of opposite sign connected to different atomic fine-structure states, $^2P_{3/2}$ and $^2P_{1/2}$, anticross [10,38,55]. The resulting curves no longer have pure C_3R^{-3} behavior, but have an additional, large C_6R^{-6} component. As an example, Ref. [10] gives $C_3=-6.2$ a.u. for the 0_g^- pure long-range potential in the Na $3^2P_{3/2}+$Na $3^2S_{1/2}$ manifold. This curve has a potential minimum $V_{\min}=-57$ GHz at $R_{\min}=71a_0$. Such a minimum occurs when the C_6 term in Eq. (15) is set equal to 1.1×10^6 a.u. This value is several orders of magnitude larger than the value of C_6 derived in Refs. [57,58]. It appears, then, that for Na, the effect of higher-energy terms on pure long-range potentials is quite small. In Ref. [57], it is mentioned that for the heavier alkali diatomic molecules, the disturbing effect of higher-energy terms becomes somewhat more significant.

A calculation of the C_6 dispersion coefficients for the excited heavy rare-gas diatomic systems would be useful, but application of the results for the alkalis is informative. A fit of our pure long-range potentials yields values of $|C_6|$ that are typically between 1 and 10×10^4 a.u. for Ne, and in the range of 5 and 50×10^4 a.u. for Kr. The values given in Ref. [57] are then at least 2% and at most 40% of our typical C_6 values. This means that qualitatively, there are no changes to our calculated potential curves. Quantitatively, a correction to our C_6 values of 10% alters the positions of $V_{\min}$ by 10% and $R_{\min}$ by about 3%, as noted in Sec. V E. The exclusion of higher-energy levels then appears to be a reasonable restriction of our basis set. In some of our restricted-basis potentials, C_6 approaches lower values, between 10^4 and 10^2 a.u. The accurate study of these cases would seem to require a larger basis set. In general, it should be emphasized that values of $V_{\min}$ and $R_{\min}$ quoted in the present work are not exact.

Xenon is an exception to the analysis given above. In Xe, the $6p'$ levels intermingle with the $7p$ levels. In this case, a useful approach might be to restrict the basis to only $6s$ and $6p$ levels, excluding the relatively distant $6p'$ states, which are about 4×10^{-2} a.u.$=8\times10^3$ cm^{-1} higher in energy than the $6p$ states.

B. Neglect of quadrupole-quadrupole interaction

In Sec. III C, we dropped the quadrupole-quadrupole interaction from our Hamiltonian, citing its relative unimportance. We will now consider this term in more detail and derive its order of magnitude for comparison with the dipole-dipole terms used exclusively until now.

The quantum mechanical expression for the quadrupole-quadrupole term is [43,67]

$$W_{q\text{-}q}=\frac{e^2}{4\pi\varepsilon_0R^5}\{Q_{1,-2}Q_{2,2}+4Q_{1,-1}Q_{2,1}+6Q_{1,0}Q_{2,0}+4Q_{1,1}Q_{2,-1}+Q_{1,2}Q_{2,-1}\}=C_5R^{-5}, \tag{22}$$

where the operator Q consists of a sum over terms from all contributing electrons, while the subscripts $-2, \ldots ,2$ denote its spherical tensor components [43,45]. The operator Q conserves parity. For the states considered in this paper, this means that all matrix elements requiring a connection between s and p states vanish:

$$_1\langle s|_2\langle p|W_{q\text{-}q}|p\rangle_1|s\rangle_2=0, \tag{23}$$

TABLE VII. Expectation values $\langle r_v^2\rangle$ and $\langle r_h^2\rangle$ for the np and ns valence electron and the $(n-1)p$ core hole for Ne ($n=3$) [68] and Kr ($n=5$) [69] together with data for the ns valence electron of the corresponding alkali atoms [69]. The $\langle r_v^2\rangle$ for Kr($5p$) was obtained by scaling the Ne($3p$) value with the ratio $\langle r_v^2\rangle$[Rb($5s$)]/$\langle r_v^2\rangle$[Na($3s$)].

Atom	n	$\langle r_h^2\rangle$ $[(n-1)p]$ (a_0^2)	$\langle r_v^2\rangle$ $[ns]$ (a_0^2)	$\langle r_v^2\rangle$ $[np]$ (a_0^2)
Ne	3	1.01	22.9	45.9
Na	3		20.7	
Kr	5	4.5		80
Rb	5		36.2	

so that only matrix elements ${}_1\langle s|_2\langle p|W_{q\text{-}q}|s\rangle_1|p\rangle_2$ need be considered. For the $s+p$ manifold we are concerned with, C_5 will thus be of order

$$C_5=\mathcal{O}\left(\frac{e^2}{4\pi\varepsilon_0}\langle r_h^2\rangle\langle r_v^2\rangle\right), \tag{24}$$

with the subscripts h and v denoting the $(n\text{-}1)p$ core hole and the np valence electron, respectively.

For Ne, we have calculated the r^2 expectation values involved from electron wave functions developed by Haberland [68]. These are displayed in Table VII, together with similar values for Kr that we have estimated based on published $\langle r^2\rangle$ values for the rare-gas and the equivalent alkali-metal atoms [69]. The table points to $C_5\approx 46$ a.u. for Ne($3s$)+Ne($3p$); a full treatment has shown that, in practice, C_5 never reaches beyond 16 a.u. in this case, due to additional Clebsch-Gordan coefficients; by scaling this gives a maximum value of $C_5=128$ a.u. for Kr. These values are of the same order of magnitude as most of the C_3 values that we have found, in which case a notable influence of the quadrupole-quadrupole term is limited to small R, where, however, the multipole expansion loses validity. We have checked that as long as $|C_3|>0.25$ a.u., the quadrupole-quadrupole term never reaches beyond 2% of the dipole-dipole term in the range $20a_0<R<1500a_0$. Even when C_3 is vanishingly small, however, the influence of the quadrupole-quadrupole term turns out to be very limited, since the C_5 values are also orders of magnitude smaller than the general C_6 values that we have developed, even to the extent that the (calculable) quadrupole-quadrupole term is smaller than the uncertainty in the induced dipole term as discussed in Sec. VII A. In fact, for Ne($3s$)+Ne($3p$), there are only two curves supporting bound states where this is not true. These two states, given by Eq. (21), have vanishing C_3 as well as particularly small $C_6\approx -5\times 10^3$ a.u.

To obtain a quantitative estimate of the relative importance of the quadrupole-quadrupole term, we have calculated the JWKB phase for all 864 Ne_2 potentials for vanishing asymptotic kinetic energy, with and without the quadrupole-quadrupole term. In all cases but two, the difference in accumulated phase in the range $20a_0<R<1500a_0$ amounts to less than 0.1π. The two exceptions, the same 2_u and 2_g states mentioned above, gave differences of 0.2π and 0.25π, respectively, on a total of 5π. While for the heavier rare gases, C_5 increases somewhat due to the larger extent of the electron orbitals, the same is true for the resonant and induced dipole-dipole interactions. For example, for Kr, C_5 values are about 7.8 times larger than for Ne, but C_3 is about two times larger and, consequently, C_6 about four times. This means that in these cases as well, the quadrupole-quadrupole interaction remains a minor effect.

C. Adiabatic corrections

The dynamical aspects of ultracold collisions taking place on the adiabatic potentials developed so far are determined by the nuclear kinetic energy operator T_R. Part of this, namely $T_R^{\text{adiab}}=-(\hbar^2/2\mu)(\partial^2/\partial R^2)$, can be incorporated in the adiabatic potentials [43]. In our case, where the lowest-order interaction has R^{-3} behavior, these adiabatic corrections conform to $T_R^{\text{adiab}}=C_8/R^8$. This comes about because the first-order correction $|\alpha'\rangle$, to the asymptotic wave functions $|\alpha\rangle$ also has R^{-3} behavior, while in addition $\langle\alpha'|\alpha\rangle=0$. Therefore adiabatic corrections are only a small perturbation at large R (we have found C_8 to be of order 4×10^6 a.u. for Ne).

VIII. CONCLUSIONS

We have determined the long-range behavior of diatomic potentials of the heavy rare gases due to the electric dipole-dipole interaction, using an approach based on experimentally measured quantities. The potentials are valid for internuclear separations from about $15a_0$ up to about $1500a_0$. Numerical calculations have been presented for diatomic states connecting asymptotically to the $R\{ns\}+R\{np\}$ separated atom limit, with $R=$ Ne and Kr, as a preliminary step towards predicting photoassociative spectra. At large internuclear separations $R\gtrsim 30a_0$ the potentials have a predominantly R^{-3} or R^{-6} behavior, while at short range they are severely complicated by anticrossings among the numerous atomic fine-structure states. A truncated basis was used to determine C_3 coefficients for the $Rns(3/2)_2+Rnp(5/2)_3$ laser cooling transition, for all $R=$ Ne, . . . ,Xe. Our calculations can easily be applied to other rare gases without hyperfine structure, and qualitatively, our results apply for them as well. One source of error in our results comes from the accuracy to which the atomic lifetimes and branching ratios are known; any error in these values linearly affects the C_3 values of our potentials. Smaller branching ratios are known with less accuracy; on the other hand, for the laser cooling transition the branching ratio is certainly 100%, so that in that case error is introduced from the value of the atomic lifetime alone. A second source of error is the exclusion of effects due to the restriction of our basis set. Particularly noteworthy is the discovery of pure long-range states in both diatomic Ne and Kr, which might be used to precisely determine atomic properties, in conjunction with spectroscopic measurements.

The multitude of potentials made it impossible to discuss all of them in detail. Interested readers are welcome to contact the authors for more specific information.

ACKNOWLEDGMENTS

We extend our gratitude to H. M. J. M. Boesten for helpful discussions. M.R.D. and J.G.C.T. thank the Netherlands Foundation for Fundamental Research on Matter (FOM) for financial support. The research of E.J.D.V. was made possible by the Royal Netherlands Academy of Arts and Sciences (KNAW).

[1] H. Metcalf and P. van der Straten, Phys. Rep. **244**, 204 (1994).
[2] P. S. Julienne and F. H. Mies, J. Opt. Soc. Am. B **6**, 2257 (1989).
[3] K. Burnett, Contemp. Phys. **37**, 1 (1996).
[4] W. Ketterle and N. van Druten, in *Evaporative Cooling of Trapped Atoms*, Vol. 37 of *Advances in Atomic, Molecular and Optical Physics*, edited by B. Bederson and H. Walther (Academic, London, 1996).
[5] K. Gibble, S. Chang, and R. Legere, Phys. Rev. Lett. **75**, 2666 (1995).
[6] J. Taylor, *Scattering Theory* (Robert E. Krieger Publishing Co. Inc., Malabar, FL, 1987).
[7] K. Burnett, P. Julienne, P. Lett, and K.-A. Suominen, Phys. World **8**, 42 (1995).
[8] J. R. Gardner *et al.*, Phys. Rev. Lett. **74**, 3764 (1995).
[9] A. J. Moerdijk and B. J. Verhaar, Phys. Rev. Lett. **73**, 518 (1994).
[10] K. M. Jones *et al.*, Europhys. Lett. **35**, 85 (1996).
[11] C. J. Williams and P. S. Julienne, J. Chem. Phys. **101**, 2634 (1994).
[12] J. Vigué, Europhys. Lett. **23**, 321 (1993).
[13] L. P. Ratliff *et al.*, J. Chem. Phys. **101**, 2638 (1994).
[14] H. R. Thorsheim, J. Weiner, and P. S. Julienne, Phys. Rev. Lett. **58**, 2420 (1987).
[15] P. D. Lett *et al.*, Phys. Rev. Lett. **71**, 2200 (1993).
[16] E. R. I. Abraham, W. I. McAlexander, H. T. C. Stoof, and R. G. Hulet, Phys. Rev. A **53**, 3092 (1996).
[17] M. R. Doery *et al.*, in *15th International Conference on Atomic Physics Zeeman-Effect Centenary* (University of Amsterdam, Amsterdam, 1996), Abstract TuH3.
[18] M. D. Hoogerland *et al.*, Appl. Phys. B: Lasers Opt. **62**, 323 (1996).
[19] M. Kumakura and N. Morita, Jpn. J. Appl. Phys., Part 2 **31**, L276 (1992).
[20] F. Shimizu, K. Shimizu, and H. Takuma, Opt. Lett. **16**, 339 (1991).
[21] W. Rooijakkers, W. Hogervorst, and W. Vassen, Opt. Commun. **135**, 149 (1997).
[22] F. Bardou *et al.*, Europhys. Lett. **20**, 30 (1992).
[23] H. Katori and F. Shimizu, Phys. Rev. Lett. **73**, 2555 (1994).
[24] M. Walhout *et al.*, Phys. Rev. Lett. **74**, 506 (1995).
[25] *Argon, Helium, and the Rare Gases*, edited by G. A. Cook (Interscience Publishers, New York, 1961).
[26] G. V. Shlyapnikov, J. T. M. Walraven, U. M. Rahmanov, and M. W. Reynolds, Phys. Rev. Lett. **73**, 3247 (1994).
[27] P. O. Fedichev, M. W. Reynolds, U. M. Rahmanov, and G. V. Shlyapnikov, Phys. Rev. A **53**, 1447 (1996).
[28] K.-A. Suominen *et al.*, Phys. Rev. A **53**, 1678 (1996).
[29] B. Brutschy and H. Haberland, J. Phys. E **10**, 90 (1977).
[30] H. Metcalf, J. Opt. Soc. Am. B **6**, 2206 (1989).
[31] A. Gallagher and D. E. Pritchard, Phys. Rev. Lett. **63**, 957 (1989).
[32] P. S. Julienne and J. Vigué, Phys. Rev. A **44**, 4464 (1991).
[33] A. A. Radzig and B. M. Smirnov, *Reference Data on Atoms, Molecules, and Ions* (Springer-Verlag, New York, 1985).
[34] M. Walhout, A. Witte, and S. L. Rolston, Phys. Rev. Lett. **72**, 2843 (1994).
[35] *Atomic Energy Levels and Grotrian Diagrams*, edited by S. Bashkin and J. O. Stoner (North-Holland Publishing Co., Amsterdam, 1975), Vol. I.
[36] V. Kaufman and C. J. Humphreys, J. Opt. Soc. Am. **59**, 1614 (1969).
[37] C. Cohen-Tannoudji, B. Diu, and F. Laloë, *Quantum Mechanics* (John Wiley & Sons, New York, 1977), Vol. II.
[38] M. Movre and G. Pichler, J. Phys. B **10**, 2631 (1977).
[39] E. I. Dashevskaya, A. I. Voronin, and E. E. Nikitin, Can. J. Phys. **47**, 1237 (1969).
[40] R. Eisberg and R. Resnick, *Quantum Physics of Atoms, Molecules, Solids, Nuclei, and Particles*, 2nd ed. (John Wiley & Sons, New York, 1985).
[41] H. B. G. Casimir and D. Polder, Phys. Rev. **73**, 360 (1948).
[42] W. J. Meath, J. Chem. Phys. **48**, 227 (1968).
[43] J. O. Hirschfelder and W. J. Meath, in *Nature of Intermolecular Forces*, Vol. XII of *Advances in Chemical Physics*, edited by J. O. Hirschfelder (Interscience Publishers, New York, 1967).
[44] H. Margenau and N. R. Kestner, *Theory of Intermolecular Forces*, 2nd ed. (Pergamon Press, New York, 1971).
[45] A. Messiah, *Quantum Mechanics* (North-Holland Publishing Co., Amsterdam, 1981), Vol. II.
[46] A. J. Moerdijk B. J. Verhaar, and A. Axelson, Phys. Rev. A **51**, R4333 (1995).
[47] G. Herzberg, *Molecular Spectra and Molecular Structure I. Spectra of Diatomic Molecules*, 2nd ed. (Van Nostrand Reinhold Co., New York, 1950).
[48] See documentation for numerical routine F02ABF in *The NAG Fortran Library Manual—Mark 16*, The Numerical Algorithms Group, Wilkinson House, Jordan Hill Rd, Oxford OX2 8DR, UK, 1996.
[49] E. Wigner and E. E. Witmer, Z. Phys. **51**, 859 (1928).
[50] See documentation for routine numerical routine E04GBF in [48].
[51] E. R. Cohen and B. N. Taylor, Phys. Today **48**(8), BG9 (1995).
[52] D. D. Konowalow, M. E. Rosencrantz, and M. L. Olson, J. Chem. Phys. **72**, 2612 (1980); G. Jeung, J. Phys. B **16**, 4289 (1983).
[53] R. L. LeRoy and R. B. Bernstein, J. Chem. Phys. **52**, 3869 (1970).
[54] W. C. Stwalley, Chem. Phys. Lett. **6**, 241 (1970).
[55] W. C. Stwalley, Y.-H. Uang, and G. Pichler, Phys. Rev. Lett. **41**, 1164 (1978).
[56] J. W. Cooley, Math. Comput. **15**, 363 (1961).
[57] B. Bussery and M. Aubert-Frécon, J. Chem. Phys. **82**, 3224 (1985).
[58] M. Marinescu and A. Dalgarno, Phys. Rev. A **52**, 311 (1995).

[59] S. A. Kandela and H. Schmoranzer, Phys. Lett. **86A**, 101 (1981).
[60] H. Schmoranzer and U. Volz, Phys. Scr. **T47**, 42 (1993).
[61] N. E. Small-Warren and L.-Y. C. Chiu, Phys. Rev. A **11**, 1777 (1975).
[62] M. V. Fonseca and J. Campos, Phys. Rev. A **17**, 1080 (1978).
[63] R. S. F. Chang, H. Horiguchi, and D. W. Setser, J. Chem. Phys. **73**, 778 (1980).
[64] P. Hartmetz and H. Schmoranzer, Z. Phys. A **317**, 1 (1984).
[65] S. Kandela, Physica B & C **123C**, 370 (1984).
[66] M. Aymar and M. Coulombe, At. Data Nucl. Data Tables **21**, 537 (1978). The branching ratios were calculated from the velocity form of the absolute transition probabilities calculated by these authors. We selected these authors' values since in general their data agreed best of all available theoretical results with the accurate lifetime data of Schmoranzer and Volz (Ref. [60]). Experimental values from several authors are listed by Chang *et al.* (Ref. [63]) but have large (30%) maximum uncertainties.
[67] T. Y. Chang, Rev. Mod. Phys. **39**, 911 (1969).
[68] H. Haberland (private communication).
[69] C. Froese Fischer, *The Hartree-Fock Method for Atoms* (John Wiley & Sons, New York, 1977).
[70] N. Gibson and J. Risley, Phys. Rev. A **52**, 4451 (1995).
[71] H. Katori and F. Shimizu, Phys. Rev. Lett. **70**, 3545 (1993). Note that Ref. [61] gives a calculated value of 85.1 s. See Ref. [34].
[72] T. Fujimoto, C. Goto, Y. Uetani, and K. Fukuda, Physica B & C **128C**, 96 (1985).
[73] C. A. Whitehead *et al.*, J. Chem. Phys. **102**, 1965 (1995). This should be compared with Ref. [62], which is older and has larger error bounds, but has more data.
[74] W. Wiese *et al.*, Phys. Rev. A **39**, 2461 (1989).
[75] C. J. Humphreys and J. E. Paul, J. Opt. Soc. Am. **60**, 1302 (1970).
[76] H. Horiguchi, R. S. F. Chang, and D. W. Setser, J. Chem. Phys. **75**, 1207 (1981).